Accepted 20th September 2018 (Immunity)

Antibodies to costimulatory receptor 4-1BB enhance anti-tumor immunity via T regulatory cell depletion and promotion of CD8 T cell effector function

Sarah L Buchan[1,8], Lang Dou[1,8], Marcus Remer[1,8], Steven G Booth[1], Stuart N Dunn[1], Chester Lai[2,3], Monika Semmrich[4], Ingrid Teige[4], Linda Mårtensson[4], Christine A Penfold[1], HT Claude Chan[1], Jane E Willoughby[1], C. Ian Mockridge[1], Lekh N Dahal[1], Kirstie LS Cleary[1], Sonya James[1], Anne Rogel[1], Päivi Kannisto[5], Mats Jernetz[5], Emily L Williams[1], Eugene Healy[2,3], J Sjef Verbeek[6], Peter WM Johnson[7], Björn Frendéus[4], Mark S Cragg[1], Martin J Glennie[1], Juliet C Gray[1,9], Aymen Al-Shamkhani[1,9,10] and Stephen A Beers[1,9,11]

[1]Antibody and Vaccine Group, Centre for Cancer Immunology, University of Southampton Faculty of Medicine, Southampton, Hants, SO16 6YD, UK. [2]Department of Dermatopharmacology, University of Southampton, Faculty of Medicine, Southampton, Hants, SO16 6YD, UK. [3]Department of Dermatology, University Hospital Southampton NHS Foundation Trust, Southampton, Hants, SO16 6YD, UK. [4]BioInvent International AB, Sölvegatan 41, 22370 Lund, SE. [5]Department of Obstetrics and Gynecology, Lund University Hospital, Lund, SE. [6]Department of Human Genetics, Leiden University Medical Centre, Leiden, NL. [7]Cancer Research UK Southampton Centre, Centre for Cancer Immunology, University of Southampton Faculty of Medicine, Southampton, Hants. SO16 6YD. [8]These authors contributed equally to this work. [9]These authors jointly supervised this work. Correspondence should be addressed to A.A-S. (A.Al-Shamkhani@soton.ac.uk), S.A.B. (sab@soton.ac.uk) or J.C.G (J.C.Gray@soton.ac.uk). [10]Senior author. [11]Lead contact.

Anti-4-1BB cancer therapy is enhanced through the engineering of dual activity mAb

SUMMARY

The costimulatory receptor 4-1BB is expressed on activated immune cells, including activated T cells. Antibodies targeting 4-1BB enhance the proliferation and survival of antigen-stimulated T cells in vitro and promote CD8 T-cell dependent anti-tumor immunity in pre-clinical cancer models. We found that T regulatory (Treg) cells infiltrating human or murine tumors expressed high amounts of 4-1BB. Intra-tumoral Treg cells were preferentially depleted by anti-4-1BB mAbs in vivo. Anti-4-1BB mAbs also promoted effector T cell agonism to promote tumor rejection. These distinct mechanisms were competitive and dependent on antibody isotype and FcγR availability. Administration of anti-4-1BB IgG2a, which preferentially depletes Treg cells, followed by either agonistic anti-4-1BB IgG1 or anti-PD-1 mAb augmented anti-tumor responses in multiple solid tumor models. An antibody engineered to optimize both FcγR-dependent Treg cell depleting capacity and FcγR-independent agonism delivered enhanced anti-tumor therapy. These insights into the effector mechanisms of anti-4-1BB mAbs lay the groundwork for translation into the clinic.

KEYWORDS

4-1BB, immunotherapy, cancer, tumor, TNFR, Treg cell, depletion, agonism, PD-1, combination.

INTRODUCTION

Immunomodulatory monoclonal antibodies (mAb), such as anti-CTLA-4, anti-PD-1/PD-L1 and anti-CD40 show positive outcomes when trialed in difficult-to-treat malignancies, albeit in a minority of patients (Beatty et al., 2011; Brahmer et al., 2012; Hodi et al., 2010; Topalian et al., 2012). These promising results reinforce the belief that the immune system holds the key to controlling cancer. Immunomodulatory mAb are directed at key molecular regulators on T cells or antigen-presenting cells (APC) and boost anti-cancer immunity through blockade of inhibitory signals (checkpoint blockers) or delivery of co-stimulatory signals (agonists). Recently this binary classification has been called into question by data showing that the therapeutic activities of T-cell targeting mAbs anti-CTLA-4, anti-GITR and anti-OX40 involve depletion of suppressive CD4+ T regulatory (Treg) cells dependent on co-engagement of activatory FcγRs (Bulliard et al., 2013; Marabelle et al., 2013; Simpson et al., 2013). The activity of agonistic APC-targeting anti-CD40 mAb, in contrast, requires co-engagement of the inhibitory FcγR to facilitate effective mAb cross-linking, which is necessary for CD40 signaling and immune stimulation (Li and Ravetch, 2011; White et al., 2011). Therefore, the mechanisms employed by immunomodulatory mAb depend on their Fab and Fc regions in ways which are ill-defined and which may depend on the cell type being targeted. Understanding the relative importance of Treg cell depletion versus direct immune-stimulation will be vital to the development and successful translation of immunomodulatory mAb to patients.

Like CD40, 4-1BB is a member of the TNFR superfamily and a promising target for cancer immunotherapy. 4-1BB is expressed following activation of CD4+ and CD8+ T cells and its ligation is required for optimal protective CD8 T-cell responses against viruses and B cell

lymphoma in mice (Middendorp et al., 2009; Snell et al., 2011). Anti-4-1BB mAb enhance the proliferation and survival of antigen-stimulated T cells in vitro and, similar to anti-CD40, promote anti-tumor immunity in pre-clinical cancer models, dependent largely on CD8 T cells (Melero et al., 2013; Snell et al., 2011). Given the agonistic nature of anti-4-1BB and the structural similarities between 4-1BB and CD40, it might be anticipated that anti-4-1BB mAb operate through a similar mechanism to anti-CD40 mAb. However, unlike CD40, 4-1BB is a downstream target of the Treg cell lineage-defining transcription factor Foxp3; it is expressed on resting Treg cells and is increased on Treg cell activation (Marson et al., 2007; McHugh et al., 2002). It is possible therefore that anti-4-1BB may act in part through the depletion of Treg cells.

Whether anti-4-1BB is a depleting or a stimulating antibody is likely to depend on its FcγR engagement and we have therefore explored the optimal isotype for therapeutic anti-4-1BB mAb in tumors. We found that although a mIgG1 isotype mAb exerted superior agonistic activity and direct immune-stimulation of CD8+ T cells, in established solid tumor settings the mIgG2a mAb provided optimal therapeutic activity due to intratumoral Treg cell depletion. However when depletion was prevented, in mice lacking activatory FcγR, the therapeutic potential of the mIgG2a was retained. Under these conditions mIgG2a was converted to an agonist by preferential engagement of the inhibitory FcγR, FcγRIIB. We further established that depletion and agonism are competing mechanisms and that engaging both simultaneously led to reduced efficacy. This blunting of activity could be overcome through sequential administration of Treg cell depleting and then immunostimulatory isotypes or through IgG-hinge engineering to produce a dual-activity anti-4-1BB mAb possessing optimal FcγR depleting capacity together with FcγR-independent agonism. These results have implications for the administration of

existing and in-development immunomodulatory mAb and for the design of next generation reagents.

RESULTS

The therapeutic activity of anti-4-1BB mAb is determined by isotype

We and others have previously established the dependence of immunostimulatory TNFR superfamily-targeting mAb on cross-linking provided by the inhibitory FcγRIIB (Li and Ravetch, 2011; White et al., 2011). To establish if this requirement similarly applies to anti-4-1BB in a solid tumor setting we generated mIgG1 and mIgG2a chimeric versions of the rIgG2a anti-4-1BB mAb (LOB12.0 generated in-house (Beers et al., 2008; Taraban et al., 2002; White et al., 2011; White et al., 2014b)). Analysis by surface plasmon resonance and flow cytometry established that these mAb possessed an expected mFcγR-binding profile, with mIgG2a having a high activatory to inhibitory FcγR-binding ratio (A:I) and conversely mIgG1 a low A:I (Fig. S1A, (Nimmerjahn and Ravetch, 2005; White et al., 2014b)); both mAb retained equivalent 4-1BB specificity and binding (Fig. S1B and C). We then assessed the therapeutic potential of these mouse anti-4-1BB mAb in three different established solid tumor models; CT26 colon carcinoma (Fig. 1A), EG7 thymoma (Fig. 1B) and NXS2 neuroblastoma (Fig. 1C). In contrast to our studies with anti-CD40 (White et al., 2011; White et al., 2014b) and published reports with other agonistic anti-TNFR superfamily mAb targeting DR5 (Haynes et al., 2010; Li and Ravetch, 2012a), the high A:I mIgG2a mAb gave considerable therapeutic benefit (80% long term survival in all three models) while the low A:I mIgG1 version delayed growth of CT26 and EG7 but failed to confer significant long-term benefit (0-20% survival). The therapeutic efficacy of mIgG2a mAb was dependent upon CD8+ T cells (Fig. S2A) and led to long-term protective anti-tumor immunity, as determined by tumor re-challenge experiments (Fig. S2B). These results show that the protective effect of mIgG2a anti-4-1BB is mediated through an adaptive anti-tumoral immune response.

4-1BB is expressed on intratumoral Treg cells in mice and humans

Having established that anti-4-1BB mIgG2a was more therapeutic than mIgG1 in treating wild-type mice with established tumors, we looked for mechanisms that could explain the immunomodulatory activity of anti-4-1BB mIgG2a. 4-1BB mRNA and protein are preferentially expressed in Treg cells compared to resting effector T cells (Elpek et al., 2007; Gavin et al., 2002; McHugh et al., 2002) and 4-1BB protein is further increased following Treg cell activation (Elpek et al., 2007; Zheng et al., 2004). Furthermore, 4-1BB is increased, at least at the transcriptional level, in intratumoral Treg cells in human solid cancers (De Simone et al., 2016; Plitas et al., 2016). We therefore examined the possibility that anti-4-1BB mIgG2a could potentiate an anti-tumor response via depletion of Treg cells. We began by confirming that 4-1BB was expressed on a substantial proportion of tumor-infiltrating Treg cells and only a small minority of effector T cells in CT26, EG7 (Fig. 2A) and NXS2 (data not shown) and found that furthermore, only a small fraction of splenic Treg cells expressed 4-1BB. To confirm that these observations are potentially translatable to humans, we determined by flow cytometry whether 4-1BB was present on intratumoral Treg cells in patients with ovarian cancer (Fig. 2B) and squamous cell carcinoma (Fig. 2C). In both cases 4-1BB was primarily on Treg cells with lower and variable expression on effector CD4+ or CD8+ T cells in tumors (Fig. 2B and C). Furthermore, 4-1BB was expressed at lower levels on Treg cells isolated from healthy PBMC, matched blood, ascites or normal skin.

4-1BB expression on intratumoral Treg cells is required for mIgG2a therapy and its depletion potential is determined by expression level

Having determined that intratumoral Treg cells express 4-1BB we used the CT26 and EG7 tumor models to investigate the depleting capacity of anti-4-1BB mAb. In wild-type CT26 tumor-bearing mice the mIgG2a mAb efficiently depleted intratumoral Treg cells, whilst the mIgG1 variant was ineffective (Fig. 3A; left panel). This depletion effect was restricted to the tumor and dependent upon expression of the Fc receptor γ chain, a crucial component of activatory FcγR complexes (Fig. 3A, left and right panels). In mice lacking expression of FcγRIIB the depleting activity of the mIgG1 mAb was significantly enhanced, demonstrating that the depletion efficiency of these mAb is intimately linked to FcγR availability and that depletion potency can be manipulated through changes in FcγR expression. Next, we sought to demonstrate definitively that 4-1BB-dependent Treg cell depletion was the main mechanism of therapeutic action of the mIgG2a isotype in solid tumors. In order to do this we generated mice expressing floxed *Tnfrsf9* on a C57BL/6 background and crossed these with mice in which the *Foxp3* gene was flanked by sequence encoding Cre recombinase (Rubtsov et al., 2008) to generate mice in which Treg cells exhibit specific genetic deletion of *Tnfrsf9* (Fig. S3A-D). We first confirmed that mice with a Treg cell specific ablation of the *Tnfrsf9* allele (*Tnfrsf9*$^{Foxp3-/-}$) lack 4-1BB expression on Treg cells but maintain levels on activated CD8 T cells in the tumor (Fig. S3C). EG7 tumors were established in these mice and Treg cell depletion in the tumor microenvironment monitored. As seen in the CT26 model mIgG2a, and not mIgG1, efficiently depleted intratumoral Treg cells in the floxed control mice but this activity was lost in mice lacking 4-1BB expression on Treg cells (Fig. 3B). Furthermore, in keeping with our contention that Treg cell depletion is the primary mechanism of action of anti-4-1BB mIgG2a, the long-term therapeutic benefit of mIgG2a was lost in mice lacking 4-1BB on Treg cells (Fig. 3C). Although when characterizing the *Tnfrsf9*$^{Foxp3-/-}$ strain we observed comparable frequencies of Treg cells throughout the lymphoid

compartment compared to WT and *Tnfrsf9*$^{fl/fl}$ controls (data not shown), the intratumoral Treg cell frequencies were reduced implying a possible role for 4-1BB in supporting intratumoral Treg cell numbers.

We next sought to formally demonstrate the depleting capacity of anti-4-1BB mAb. Using WT mouse bone-marrow-derived macrophages and 4-1BB-expressing T cell targets we observed that mIgG2a induced effective phagocytosis of target cells whereas the mIgG1 mAb was ineffective (Fig. 3D). In agreement with our in vivo depletion results (Fig. 3A) when *Fcgr2b*$^{-/-}$ macrophages were used as effectors a significant increase in mIgG1-mediated phagocytosis was observed (Fig. 3D) in line with levels obtained with mIgG2a and WT effectors. To confirm the translational potential of our findings we additionally used human target cells and monocyte-derived macrophage effectors. In this system we found that two different anti-human 4-1BB clones (SAP3-6 and 005-B02; both of hIgG1 isotype and with A:I FcγR-binding ratios comparable to anti-4-1BB mIgG2a, (Vonderheide and Glennie, 2013)) could mediate effective phagocytic clearance (Fig. 3E, left). We then sought to confirm that the level of 4-1BB expression rather than the cell type per se dictated the efficacy of depletion. We did this using both human (Fig. 3E, right) and mouse (data not shown) in vitro generated macrophages and target cells with varying levels of 4-1BB expression and found a direct correlation between the level of 4-1BB expression on target cells and the efficiency of target-cell depletion. Finally, we tested the depletion efficiency of anti-4-1BB mAbs on human T cell targets in vivo. Human PBMC transferred to the peritoneal cavity of immunocompromised mice became activated and expressed 4-1BB. In this setting CD127 low CD25 high Treg cells expressed significantly higher levels of 4-1BB than CD8+ T cells (Fig. 3F) mirroring levels seen in human tumors (Fig. 2B and

C). When human IgG1 anti-human 4-1BB mAb were administered to these mice significant and preferential depletion of Treg cells versus CD8+ T cells was observed (Fig. 3G). Taken together these data support the contention that the high level of 4-1BB expressed on Treg cells in the tumor microenvironment makes them more susceptible to 4-1BB-dependent depletion compared with lower expressing CD8+ cells.

The role of FcγR in mediating the anti-tumor activity of anti-4-1BB mAb

As anti-4-1BB mIgG2a efficiently depleted intratumoral Treg cells dependent on activatory FcγR, we reasoned that the absence of activatory FcγR would be detrimental for the therapeutic effects of this mAb in solid tumor models. However, anti-4-1BB mIgG2a retained anti-tumor activity in the absence of activatory FcγR (i.e. in *Fcer1g*$^{-/-}$ mice; Fig. 4A and B; CT26 and EG7, respectively), suggesting that Treg cell depletion may not fully account for its therapeutic activity. In contrast to the minimal effects on anti-4-1BB mIgG2a efficacy, there was a substantial improvement in the ability of anti-4-1BB mIgG1 to promote anti-tumor immunity in the absence of activatory FcγR in both models. These findings suggest that in the absence of competitive binding of mAb to activatory FcγR, both mIgG1 and mIgG2a engage FcγRIIB efficiently, likely allowing optimal cross-linking of mAb to deliver costimulation. In keeping with the enhanced Tregcell depleting activity of mIgG1 in *Fcgr2b*$^{-/-}$ mice (Fig. 3A) the mIgG1 isotype mAb demonstrated equivalent activity to mIgG2a in *Fcgr2b*$^{-/-}$ mice (Fig. 4A). These results, coupled with the observation that in the absence of all FcγR (*Fcer1g*$^{-/-}$;*Fcgr2b*$^{-/-}$), neither mAb produced any therapeutic activity (Fig. 4A), underscore the importance of efficient, non-competing FcγR engagement for optimal in vivo activity.

CD8 T cell immunostimulatory activity of anti-4-1BB is optimal as a mouse IgG1 isotype

We next sought to establish the isotype-dependence of anti-4-1BB mAb agonist activity in vitro and in vivo. Using in vitro T-cell co-stimulation assays (Fig. 5A and Fig. S4) mIgG1 demonstrated superior agonistic activity compared with mIgG2a, in keeping with published results using other TNFR superfamily targeting mAb (White et al., 2011; White et al., 2014b). The costimulatory activity observed for mIgG1 was independent of Treg cells (Fig. 5A), suggesting that this anti-4-1BB mAb mediates its effects through targeting 4-1BB on effector T cells. Further, the costimulatory activity of mIgG1 was abolished by the addition of mIgG2a (Fig. 5B), confirming that both mAb variants bind with similar avidity and compete for binding to 4-1BB on effector T cells (Fig. S1B and Fig. 5B). These in vitro results were confirmed using an in vivo immunization model with the model antigen OVA in both an endogenous (Fig. 5C; left panel) and an OT1 T-cell transfer setting (Fig. S5A). In this context the superior agonistic activity of mIgG1 was dependent upon the inhibitory FcγRIIB (Fig. 5C right panel and Fig. S5A) as previously shown for anti-CD40 mAb (Mimoto et al., 2013; White et al., 2015; White et al., 2011; White et al., 2014b). Similarly, and in support of the in vivo therapy observed by mIgG2a mAb in *Fcer1g*$^{-/-}$ mice (Fig. 4A and B), agonistic activity of mIgG2a was revealed in treated *Fcer1g*$^{-/-}$ animals (Fig. 5C right panel). These data demonstrate that mechanisms with differential FcγR requirements effectively compete with each other and the therapeutic outcome of mAb treatment is dependent on mAb Fc binding profiles and FcγR availability.

Having established that mIgG1 was the optimal isotype for agonistic activity we wanted to establish whether this agonistic activity was mediated through direct immune activation of 4-1BB-expressing CD8+ T cells. In order to do this we generated a full *Tnfrsf9*$^{-/-}$ mouse model on a

C57BL/6 background (Fig. S3A) and transferred in purified OT-1 CD8+ T cells which were WT for *Tnfrsf9* and therefore express 4-1BB under normal physiological regulation. These mice were then challenged with OVA and anti-4-1BB mAb. In keeping with the results in WT 4-1BB expressing mice (Fig. 5C and Fig. S5A) we observed that anti-4-1BB mIgG1 produced a robust tetramer positive CD8+ T-cell response when 4-1BB expression was restricted to CD8+ T cells (Fig. 5D) supporting our contention that 4-1BB costimulatory activity is induced through direct activation of CD8+ T cells.

We next sought to determine if we could observe activation of tumor infiltrating CD8+ T cells in mIgG1 and mIgG2a treated CT26 and EG7 tumor bearing mice. Administration of mIgG1 or mIgG2a mAb to tumor-bearing mice led to an increase in tumor-infiltrating CD8+ T cells expressing Ki-67 and KLRG1 in the CT26 and EG7 tumor models, respectively (Fig. 5E and 5F) although the increase induced by the mIgG2a isotype was significantly less than that driven by mIgG1. Notably, mIgG1-dependent CD8 T cell agonistic effects were not affected by the loss of 4-1BB on Treg cells (Fig. 5F) supporting the notion that this activity is mediated through direct activation of the CD8+ T cells.

Finally, we used two vaccination strategies (tyrosine hydroxylase peptide with the NXS2 tumor or irradiated B16/BL6 cells engineered to secrete a form of Flt3L (FVAX); Fig. 5G, right panel and Fig. S5B respectively) to increase the therapeutic effect of mIgG1 and found that in these immune-primed settings that both mIgG1 and mIgG2a isotype mAbs were equally therapeutic. Of note, the efficacy of mIgG1, but not mIgG2a, was abolished in the absence of vaccination (Fig. 5G, left panel). Taken together these data confirm that mIgG1, but not mIgG2a, operates

primarily through a mechanism dependent on FcγRIIB cross-linking and direct immune activation of CD8+ T cells.

Sequential administration of Treg-cell depleting and immunostimulatory mAb leads to enhanced anti-cancer therapy

Our results demonstrating that the therapeutic activities of isotype variants of anti-4-1BB mAb occur via different mechanisms indicated a potential for combined use to enhance therapy. However, since depletion of Treg cells (mIgG2a) and delivery of costimulation (mIgG1) both relied on engagement of FcγRs, and appeared to do so in a competitive manner, we speculated that sequential rather than concurrent administration might be optimal. We therefore compared the therapeutic effect of concurrent and sequential administration of anti-4-1BB mIgG2a and mIgG1 mAb. As previously observed the mIgG2a, but not mIgG1, variant was active as a single agent (Fig. 6A). Concurrent administration of mIgG2a and mIgG1 anti-4-1BB mAb resulted in reduced therapeutic efficacy as indicated by increased tumor size (Fig. 6A) and reduced frequency of tumor free mice (Fig. 6B) compared to mIgG2a single agent treatment. In contrast, sequential delivery of first mIgG2a, to deplete Treg cells, followed 4 days later by agonistic mIgG1 to provide costimulation, improved both tumor control and the frequency of tumor-free mice (Fig. 6A and B). These findings demonstrate that the therapeutic efficacy of FcγR-dependent immunomodulatory mAb can be optimized by sequential administration and indicate that 4-1BB-mediated Treg cell depletion may have broad utility to improve the efficacy of other immune-modulatory antibodies, including checkpoint blockers.

We therefore investigated the therapeutic potential of combining Treg-cell depleting anti-4-1BB with an antibody targeting the PD-1 checkpoint receptor. We reduced the dosing of mIgG2a mAb to obtain suboptimal monotherapy and then combined anti-4-1BB mIgG2a sequentially with a deglycosylated variant anti-PD-1 blocking antibody, incapable of binding FcγRs (Tipton et al., 2015) (Fig. S6A and B) and which therefore mimics the poor FcγR-engagement of clinically-validated anti-PD-1 antibodies nivolumab and pembrolizumab (Dahan et al., 2015). This combination produced a significant increase in therapy leading to 80% long-term responders compared with 20 – 25% with either monotherapy (Figure 6C). The combination of anti-4-1BB mIgG1 and wild-type anti-PD-1 did not enhance responses compared with either monotherapy, demonstrating that for optimal combination therapies it is vital to understand the impact of isotype and scheduling of each component of any combination.

Anti-4-1BB mIgG2a/h2B engineered to possess dual activity delivers augmented cancer therapy

We next investigated if it is possible to effect both agonism and depletion through the engineering of a single mAb. Given that mAb-mediated Treg cell depletion and immunostimulatory agonism have differential and competing FcγR requirements we sought to capitalize on our previous finding that the human IgG2 hinge region is able to impart anti-TNFR superfamily member mAb with FcγR-independent agonistic properties (White et al., 2015). Here, we cloned the human IgG2 CH1 and hinge-region into the murine mIgG2a constant regions of anti-4-1BB as detailed previously (White et al., 2015) and then skewed the hinge to the agonism-enhanced ‘B’ form to make anti-4-1BB mIgG2a/h2B (Fig S7A and Fig. 7A). When tested in vitro mIgG2a/h2B had significantly enhanced agonistic activity compared to the

mIgG2a parental mAb (Fig. 7B), despite an unchanged FcγR binding profile (Fig. S7B). Despite this enhanced agonistic activity the engineered mAb also retained strong phagocytic potential in vitro (Fig. 7C). Finally, we compared this mAb with the parental mIgG2a in vivo and found that the dual activity mIgG2a/h2B had equally potent Treg-cell depleting capacity as the parental mIgG2a but now also possessed marked CD8 T-cell stimulating capability leading to an enhanced intratumoral CD8/Treg cell ratio (Fig. 7D). This dual-activity mAb also demonstrated greater therapeutic potential curing 86% of mice compared to 53% with the standard mIgG2a (Fig. 7E). These data demonstrate that a single mAb can be engineered to optimally mediate depletion and agonism, and through this enhanced dual activity deliver better therapy.

DISCUSSION

It has been established in a variety of in vitro and in vivo models that anti-TNFR superfamily mAb require efficient cross-linking to induce their agonistic effects and for most mAb this is best achieved by inhibitory FcγR engagement (Li and Ravetch, 2011, 2012a, b; White et al., 2011; White et al., 2014b). Despite these findings, it is not clear whether direct agonism is the main mechanism of therapeutic activity of these mAb in a solid tumor setting. We have investigated this question using mIgG2a and mIgG1 isotype anti-4-1BB mAb, which have a high and low activatory:inhibitory FcγR-binding ratio, and consequently good depleting and agonistic potential, respectively (White et al., 2014a).

We found using three different solid tumor models in different wild-type strains of mice that mIgG2a mAb produced substantial therapeutic effects whereas mIgG1 was less effective. The mIgG2a-dependent therapeutic activity displayed in these different tumor models suggested that therapy was likely mediated by an effector-cell dependent depletion mechanism. None of the tumors used were 4-1BB positive (data not shown) meaning this could not be a direct tumor-targeting effect as seen for anti-CD20 mAb (Minard-Colin et al., 2008).

Given the recent findings that mAb targeting CTLA-4, OX40 and GITR are able to mediate therapy through intratumoral Treg cell depletion (Bulliard et al., 2013; Marabelle et al., 2013; Simpson et al., 2013) we examined 4-1BB expression in these models and found it to be highly expressed on intratumoral Treg cells. Importantly for the potential translation of these findings to humans we found that 4-1BB demonstrated restricted expression on intratumoral Treg cells in patients with both ovarian cancer and squamous cell carcinoma supporting the therapeutic

potential of this approach in patients. Furthermore, mIgG2a depleted this suppressive population in an activatory FcγR-dependent manner, whilst mIgG1 had little effect. In keeping with the requirement for a high activatory to inhibitory FcγR-binding ratio for productive depletion, when these experiments were carried out in *Fcgr2b*$^{-/-}$ mice mIgG1 exhibited comparable depleting capacity to mIgG2a both in vivo and in vitro. Treg cell depletion was as a result of direct targeting as mice deficient for 4-1BB on Treg cells were resistant to depletion and the mIgG2a therapeutic effect was diminished in these mice. Treg-cell specific depletion appeared to simply result from higher 4-1BB expression on Treg cells as compared to CD8+ T cells rather than cell specific susceptibility or resistance and led to selective depletion of mouse and human Treg cells in vivo.

Although Treg cell depletion was the most effective mechanism of action for 4-1BB mAb in these models, we postulated that in the absence of competition for binding with activatory FcγR these mAb may produce a therapeutic effect through their agonistic function. We tested this using the CT26 and EG7 models in *Fcer1g*$^{-/-}$ mice and found that in the absence of activatory FcγR, mIgG1 mAb did become therapeutic. It was also notable, and in keeping with our contention that 4-1BB has a relatively low threshold for cross-linking in vivo, that in the absence of activatory FcγR, mIgG2a also retained activity. In agreement with the enhanced Treg-cell depleting activity of mIgG1 in *Fcgr2b*$^{-/-}$ mice when therapies were carried out in *Fcgr2b*$^{-/-}$ mice bearing CT26 tumors the mIgG1 isotype mAb demonstrated enhanced and equivalent activity to mIgG2a. Neither mAb was able to protect mice in the complete absence of FcγR demonstrating both agonistic and depletion mechanisms to be FcγR dependent.

The depletion-dependent effects discussed above were in marked contrast to the agonistic activity of these mAb on CD8+ T cells, where mIgG1 was more effective. In contrast to previous publications with anti-CD40 mAb, anti-4-1BB mIgG2a was not without direct T-cell agonistic activity in vitro and in vivo, suggesting that 4-1BB may possess a lower crosslinking threshold for signaling than CD40 (White et al., 2011; White et al., 2014b).

The fact that anti-4-1BB mAb could be therapeutic using two separate mechanisms, given the provision of the appropriate FcγR, suggests that both mechanisms could be engaged if mAb were administered sequentially. Indeed this was found to be the case when mIgG2a was given first to deplete Treg cells and then mIgG1 given to deliver an agonistic signal; when mAb were administered simultaneously then little therapeutic effect was evident. These observations support the hypothesis that simultaneous engagement of these two FcγR-dependent mechanisms through the engagement of a single antigen may not be possible but that temporal, as shown here, or potentially spatial (intratumor versus systemic) separation of these mAb may facilitate their combined efficacy.

In order to further demonstrate the likely isotype and scheduling requirements for anti-4-1BB mAb in patients, where clinical results suggest combination approaches are likely to be required, we investigated different mAb combinations with anti-PD-1. In this setting we found that isotype-optimal versions of both anti-4-1BB and anti-PD-1 produced a significant combination effect leading to cures in 80% of mice treated.

In the clinic there has been much interest in targeting 4-1BB using agonistic antibodies. Our finding that 4-1BB expression was more abundant on intratumoral Treg cells than CD8 T cells and that anti-41BB mAb specifically deleted Treg cells in animal models suggests that this strategy may be particularly appealing in patients. In support of the potential of this approach two small clinical studies have reported a correlation between Treg cell depletion in tumors and therapeutic response to anti-CTLA-4 mAb therapy (Romano et al., 2015; Arce Vargas et al., 2018).

Currently two fully humanized anti-4-1BB mAbs are in development; urelumab (BMS-663513), an IgG4 antibody manufactured by Bristol-Myers Squibb, and utomilumab (PF-05082566), a fully humanized IgG2 produced by Pfizer. Thus far utomilumab has proven safe causing only grade 1 toxicities in patients (Segal et al., 2014) whereas urelumab caused adverse effects in 15% of patients including increased liver enzymes, pruritus and diarrhea (Molckovsky and Siu, 2008). Despite their promising safety profiles, neither urelumab or utomilumab are predicted to strongly bind FcγRIIB or deplete Treg cells calling into question whether either antibody will prove effective in patients (Furness et al., 2014). Data from our group show that a human IgG2 antibody targeting 4-1BB can act as a superagonist independent of FcγR and it remains possible that utomilumab might act in a similar manner (White et al., 2015). Alternatively, the data presented herein demonstrating improved efficacy of Treg-cell depleting compared with immune-agonist variant anti-4-1BB antibodies, and selective intratumoral 4-1BB expression on Treg cells compared with CD8+ effector cells, support development of human therapeutic anti-4-1BB isotype antibodies selected for their capacity to deplete Treg cells (Furness et al., 2014). Our data support findings recently reported in Arce Vargas et al, indicating that Treg-cell

depleting antibodies may synergize with checkpoint blockade to boost responses, and help overcome resistance (Arce Vargas et al., 2017).

Our findings to this point support the contention that immunomodulatory mAb can harness multiple mechanisms of action for therapy and we wanted to test the possibility that a single antibody could be engineered to carry out both depletion and agonism. Given our data demonstrating the competing FcγR requirements for these mechanisms in vitro and in vivo it seemed unlikely that engineering a mAb to possess enhanced activatory and inhibitory FcγR engagement would work given that any one mAb can only engage a single FcγR at a time. Given these potential limitations we generated a mIgG2a mAb with optimal depleting capacity to incorporate the hIgG2 hinge region which we skewed to the agonism-optimal 'B' form. We hypothesized that this mAb would be able to perform both functions and found this to be the case both in vitro and in vivo; this mAb also led to enhanced therapy in a solid tumor model. These results have direct implications for the administration of existing and in-development immunomodulatory mAb and potentially for the design and development of next-generation reagents and strategies for their use.

ACKNOWLEDGEMENTS

We are grateful to Alison Tutt and the staff of the University of Southampton Biomedical Research facility for their technical support. We are grateful to Prof Dieter Riethmacher for providing access to Flp delete mice (B6.129S4-*Gt(ROSA)26Sor*$^{tm1(FLP1)Dym}$/RainJ) and for technical help with genotyping. We also thank Leon Douglas and Patrick Duriez from the ECMC/CRUK Protein Core Facility for making SIINFEKL tetramers and human M-CSF respectively. This work was funded by Cancer Research UK (grants C34592/A12343, C1477/A10834, C8574/A11781 and C34999A/A18087), Bloodwise (12050 and 12020) and the FP6 Marie Curie Research Training Network Immune Deficient Mice (MRTN-CT-2004-005632). CL is a Wellcome Trust Research Training Fellow.

AUTHOR CONTRIBUTIONS

S.L.B., L.D., M.R., S.G.B., S.N.D., M.S., I.T., L.M., C.A.P, J.E.W., C.I.M., L.N.D., K.L.C., S.J., A.R. and E.L.W. performed experiments and interpreted the data; C.L., P.K., M.J. and E.H. provided and analyzed the clinical data; S.N.D., H.T.C.C, I.T., E.L.W., B.F. and J.S.V. provided key materials; S.A.B., S.L.B., J.C.G. and A.A-S. wrote the manuscript; P.W.M.J., B.F., M.S.C. and M.J.G. helped design the study, interpreted data and revised the manuscript; S.A.B., J.C.G. and A.A-S. designed the study, interpreted the data and supervised the project.

DECLARATION OF INTEREST

M.S., I.T., and B.F. are employees of BioInvent International. K.L.C. received funding from BioInvent. M.S.C. acts as a consultant to BioInvent and has received institutional support from BioInvent for grants and patents. J.C.G. has received institutional support for a grant from BioInvent. M.J.G. and S.A.B. have received institutional support from BioInvent for grants and

patents. M.S., I.T.,L.M., B.F., M.J.G., J.C.G., A.A-S. and S.A.B. have a patent application filed in relation to this work.

REFERENCES

Arce Vargas, F., Furness, A.J.S., Litchfield, K., Joshi, K., Rosenthal, R., Ghorani, E., Solomon, I., Lesko, M.H., Ruef, N., Roddie, C., *et al.* (2018). Fc Effector Function Contributes to the Activity of Human Anti-CTLA-4 Antibodies. Cancer cell *33*, 649-663 e644.

Arce Vargas, F., Furness, A.J.S., Solomon, I., Joshi, K., Mekkaoui, L., Lesko, M.H., Miranda Rota, E., Dahan, R., Georgiou, A., Sledzinska, A., *et al.* (2017). Fc-Optimized Anti-CD25 Depletes Tumor-Infiltrating Regulatory T Cells and Synergizes with PD-1 Blockade to Eradicate Established Tumors. Immunity *46*, 577-586.

Beatty, G.L., Chiorean, E.G., Fishman, M.P., Saboury, B., Teitelbaum, U.R., Sun, W., Huhn, R.D., Song, W., Li, D., Sharp, L.L., *et al.* (2011). CD40 agonists alter tumor stroma and show efficacy against pancreatic carcinoma in mice and humans. Science *331*, 1612-1616.

Beers, S.A., Chan, C.H., James, S., French, R.R., Attfield, K.E., Brennan, C.M., Ahuja, A., Shlomchik, M.J., Cragg, M.S., and Glennie, M.J. (2008). Type II (tositumomab) anti-CD20 monoclonal antibody out performs type I (rituximab-like) reagents in B-cell depletion regardless of complement activation. Blood *112*, 4170-4177.

Beers, S.A., French, R.R., Chan, H.T., Lim, S.H., Jarrett, T.C., Vidal, R.M., Wijayaweera, S.S., Dixon, S.V., Kim, H., Cox, K.L., *et al.* (2010). Antigenic modulation limits the efficacy of anti-CD20 antibodies: implications for antibody selection. Blood *115*, 5191-5201.

Brahmer, J.R., Tykodi, S.S., Chow, L.Q., Hwu, W.J., Topalian, S.L., Hwu, P., Drake, C.G., Camacho, L.H., Kauh, J., Odunsi, K., *et al.* (2012). Safety and activity of anti-PD-L1 antibody in patients with advanced cancer. The New England journal of medicine *366*, 2455-2465.

Buchan, S.L., and Al-Shamkhani, A. (2012). Distinct motifs in the intracellular domain of human CD30 differentially activate canonical and alternative transcription factor NF-kappaB signaling. PloS one *7*, e45244.

Bulliard, Y., Jolicoeur, R., Windman, M., Rue, S.M., Ettenberg, S., Knee, D.A., Wilson, N.S., Dranoff, G., and Brogdon, J.L. (2013). Activating Fc gamma receptors contribute to the antitumor activities of immunoregulatory receptor-targeting antibodies. The Journal of experimental medicine *210*, 1685-1693.

Curran, M.A., and Allison, J.P. (2009). Tumor vaccines expressing flt3 ligand synergize with ctla-4 blockade to reject preimplanted tumors. Cancer research *69*, 7747-7755.

Dahan, R., Sega, E., Engelhardt, J., Selby, M., Korman, A.J., and Ravetch, J.V. (2015). FcgammaRs Modulate the Anti-tumor Activity of Antibodies Targeting the PD-1/PD-L1 Axis. Cancer cell *28*, 285-295.

De Simone, M., Arrigoni, A., Rossetti, G., Gruarin, P., Ranzani, V., Politano, C., Bonnal, R.J., Provasi, E., Sarnicola, M.L., Panzeri, I., *et al.* (2016). Transcriptional Landscape of Human Tissue Lymphocytes Unveils Uniqueness of Tumor-Infiltrating T Regulatory Cells. Immunity *45*, 1135-1147.

Elpek, K.G., Yolcu, E.S., Franke, D.D., Lacelle, C., Schabowsky, R.H., and Shirwan, H. (2007). Ex vivo expansion of CD4+CD25+FoxP3+ T regulatory cells based on synergy between IL-2 and 4-1BB signaling. Journal of immunology *179*, 7295-7304.

French, R.R., Chan, H.T., Tutt, A.L., and Glennie, M.J. (1999). CD40 antibody evokes a cytotoxic T-cell response that eradicates lymphoma and bypasses T-cell help. Nature medicine *5*, 548-553.

Furness, A.J., Vargas, F.A., Peggs, K.S., and Quezada, S.A. (2014). Impact of tumour microenvironment and Fc receptors on the activity of immunomodulatory antibodies. Trends in immunology *35*, 290-298.
Gavin, M.A., Clarke, S.R., Negrou, E., Gallegos, A., and Rudensky, A. (2002). Homeostasis and anergy of CD4(+)CD25(+) suppressor T cells in vivo. Nature immunology *3*, 33-41.
Haynes, N.M., Hawkins, E.D., Li, M., McLaughlin, N.M., Hammerling, G.J., Schwendener, R., Winoto, A., Wensky, A., Yagita, H., Takeda, K., *et al.* (2010). CD11c+ dendritic cells and B cells contribute to the tumoricidal activity of anti-DR5 antibody therapy in established tumors. Journal of immunology *185*, 532-541.
Hodi, F.S., O'Day, S.J., McDermott, D.F., Weber, R.W., Sosman, J.A., Haanen, J.B., Gonzalez, R., Robert, C., Schadendorf, D., Hassel, J.C., *et al.* (2010). Improved survival with ipilimumab in patients with metastatic melanoma. The New England journal of medicine *363*, 711-723.
Li, F., and Ravetch, J.V. (2011). Inhibitory Fcgamma receptor engagement drives adjuvant and anti-tumor activities of agonistic CD40 antibodies. Science *333*, 1030-1034.
Li, F., and Ravetch, J.V. (2012a). Apoptotic and antitumor activity of death receptor antibodies require inhibitory Fcgamma receptor engagement. Proceedings of the National Academy of Sciences of the United States of America *109*, 10966-10971.
Li, F., and Ravetch, J.V. (2012b). A general requirement for FcgammaRIIB co-engagement of agonistic anti-TNFR antibodies. Cell cycle *11*, 3343-3344.
Lim, S.H., Vaughan, A.T., Ashton-Key, M., Williams, E.L., Dixon, S.V., Chan, H.T., Beers, S.A., French, R.R., Cox, K.L., Davies, A.J., *et al.* (2011). Fc gamma receptor IIb on target B cells promotes rituximab internalization and reduces clinical efficacy. Blood *118*, 2530-2540.
Lode, H.N., Xiang, R., Varki, N.M., Dolman, C.S., Gillies, S.D., and Reisfeld, R.A. (1997). Targeted interleukin-2 therapy for spontaneous neuroblastoma metastases to bone marrow. Journal of the National Cancer Institute *89*, 1586-1594.
Marabelle, A., Kohrt, H., Sagiv-Barfi, I., Ajami, B., Axtell, R.C., Zhou, G., Rajapaksa, R., Green, M.R., Torchia, J., Brody, J., *et al.* (2013). Depleting tumor-specific Tregs at a single site eradicates disseminated tumors. The Journal of clinical investigation *123*, 2447-2463.
Marson, A., Kretschmer, K., Frampton, G.M., Jacobsen, E.S., Polansky, J.K., MacIsaac, K.D., Levine, S.S., Fraenkel, E., von Boehmer, H., and Young, R.A. (2007). Foxp3 occupancy and regulation of key target genes during T-cell stimulation. Nature *445*, 931-935.
McHugh, R.S., Whitters, M.J., Piccirillo, C.A., Young, D.A., Shevach, E.M., Collins, M., and Byrne, M.C. (2002). CD4(+)CD25(+) immunoregulatory T cells: gene expression analysis reveals a functional role for the glucocorticoid-induced TNF receptor. Immunity *16*, 311-323.
Melero, I., Hirschhorn-Cymerman, D., Morales-Kastresana, A., Sanmamed, M.F., and Wolchok, J.D. (2013). Agonist antibodies to TNFR molecules that costimulate T and NK cells. Clinical cancer research : an official journal of the American Association for Cancer Research *19*, 1044-1053.
Middendorp, S., Xiao, Y., Song, J.Y., Peperzak, V., Krijger, P.H., Jacobs, H., and Borst, J. (2009). Mice deficient for CD137 ligand are predisposed to develop germinal center-derived B-cell lymphoma. Blood *114*, 2280-2289.
Mimoto, F., Katada, H., Kadono, S., Igawa, T., Kuramochi, T., Muraoka, M., Wada, Y., Haraya, K., Miyazaki, T., and Hattori, K. (2013). Engineered antibody Fc variant with selectively enhanced FcgammaRIIb binding over both FcgammaRIIa(R131) and FcgammaRIIa(H131). Protein engineering, design & selection : PEDS *26*, 589-598.

Minard-Colin, V., Xiu, Y., Poe, J.C., Horikawa, M., Magro, C.M., Hamaguchi, Y., Haas, K.M., and Tedder, T.F. (2008). Lymphoma depletion during CD20 immunotherapy in mice is mediated by macrophage FcgammaRI, FcgammaRIII, and FcgammaRIV. Blood *112*, 1205-1213.
Molckovsky, A., and Siu, L.L. (2008). First-in-class, first-in-human phase I results of targeted agents: highlights of the 2008 American society of clinical oncology meeting. Journal of hematology & oncology *1*, 20.
Moore, M.W., Carbone, F.R., and Bevan, M.J. (1988). Introduction of soluble protein into the class I pathway of antigen processing and presentation. Cell *54*, 777-785.
Nimmerjahn, F., and Ravetch, J.V. (2005). Divergent immunoglobulin g subclass activity through selective Fc receptor binding. Science *310*, 1510-1512.
Plitas, G., Konopacki, C., Wu, K., Bos, P.D., Morrow, M., Putintseva, E.V., Chudakov, D.M., and Rudensky, A.Y. (2016). Regulatory T Cells Exhibit Distinct Features in Human Breast Cancer. Immunity *45*, 1122-1134.
Romano, E., Kusio-Kobialka, M., Foukas, P.G., Baumgaertner, P., Meyer, C., Ballabeni, P., Michielin, O., Weide, B., Romero, P., and Speiser, D.E. (2015). Ipilimumab-dependent cell-mediated cytotoxicity of regulatory T cells ex vivo by nonclassical monocytes in melanoma patients. Proceedings of the National Academy of Sciences of the United States of America *112*, 6140-6145.
Rubtsov, Y.P., Rasmussen, J.P., Chi, E.Y., Fontenot, J., Castelli, L., Ye, X., Treuting, P., Siewe, L., Roers, A., Henderson, W.R., Jr., *et al.* (2008). Regulatory T cell-derived interleukin-10 limits inflammation at environmental interfaces. Immunity *28*, 546-558.
Segal, N.H., Gopal, A.K., Bhatia, S., Kohrt, H., Levy, R., Pishvaian, M.J., Houot, R., Bartlett, N., Nghiem, N., Kronenberg, S.A., *et al.* (2014). A phase 1 study of PF-05082566 (anti-4-1BB) in patients with advanced cancer. Journal of clinical oncology : official journal of the American Society of Clinical Oncology *32*, suppl; abstr 3007.
Simpson, T.R., Li, F., Montalvo-Ortiz, W., Sepulveda, M.A., Bergerhoff, K., Arce, F., Roddie, C., Henry, J.Y., Yagita, H., Wolchok, J.D., *et al.* (2013). Fc-dependent depletion of tumor-infiltrating regulatory T cells co-defines the efficacy of anti-CTLA-4 therapy against melanoma. The Journal of experimental medicine *210*, 1695-1710.
Snell, L.M., Lin, G.H., McPherson, A.J., Moraes, T.J., and Watts, T.H. (2011). T-cell intrinsic effects of GITR and 4-1BB during viral infection and cancer immunotherapy. Immunological reviews *244*, 197-217.
Taraban, V.Y., Rowley, T.F., O'Brien, L., Chan, H.T., Haswell, L.E., Green, M.H., Tutt, A.L., Glennie, M.J., and Al-Shamkhani, A. (2002). Expression and costimulatory effects of the TNF receptor superfamily members CD134 (OX40) and CD137 (4-1BB), and their role in the generation of anti-tumor immune responses. European journal of immunology *32*, 3617-3627.
Tipton, T.R., Mockridge, C.I., French, R.R., Tutt, A.L., Cragg, M.S., and Beers, S.A. (2015). Anti-mouse FcgammaRIV antibody 9E9 also blocks FcgammaRIII in vivo. Blood *126*, 2643-2645.
Topalian, S.L., Hodi, F.S., Brahmer, J.R., Gettinger, S.N., Smith, D.C., McDermott, D.F., Powderly, J.D., Carvajal, R.D., Sosman, J.A., Atkins, M.B., *et al.* (2012). Safety, activity, and immune correlates of anti-PD-1 antibody in cancer. The New England journal of medicine *366*, 2443-2454.
Vonderheide, R.H., and Glennie, M.J. (2013). Agonistic CD40 antibodies and cancer therapy. Clinical cancer research : an official journal of the American Association for Cancer Research *19*, 1035-1043.

White, A.L., Beers, S.A., and Cragg, M.S. (2014a). FcgammaRIIB as a key determinant of agonistic antibody efficacy. Current topics in microbiology and immunology *382*, 355-372.
White, A.L., Chan, H.T., French, R.R., Willoughby, J., Mockridge, C.I., Roghanian, A., Penfold, C.A., Booth, S.G., Dodhy, A., Polak, M.E., *et al.* (2015). Conformation of the human immunoglobulin G2 hinge imparts superagonistic properties to immunostimulatory anticancer antibodies. Cancer cell *27*, 138-148.
White, A.L., Chan, H.T., Roghanian, A., French, R.R., Mockridge, C.I., Tutt, A.L., Dixon, S.V., Ajona, D., Verbeek, J.S., Al-Shamkhani, A., *et al.* (2011). Interaction with FcgammaRIIB is critical for the agonistic activity of anti-CD40 monoclonal antibody. Journal of immunology *187*, 1754-1763.
White, A.L., Dou, L., Chan, H.T., Field, V.L., Mockridge, C.I., Moss, K., Williams, E.L., Booth, S.G., French, R.R., Potter, E.A., *et al.* (2014b). Fcgamma receptor dependency of agonistic CD40 antibody in lymphoma therapy can be overcome through antibody multimerization. Journal of immunology *193*, 1828-1835.
Wypych, J., Li, M., Guo, A., Zhang, Z., Martinez, T., Allen, M.J., Fodor, S., Kelner, D.N., Flynn, G.C., Liu, Y.D., *et al.* (2008). Human IgG2 antibodies display disulfide-mediated structural isoforms. The Journal of biological chemistry *283*, 16194-16205.
Zheng, G., Wang, B., and Chen, A. (2004). The 4-1BB costimulation augments the proliferation of CD4+CD25+ regulatory T cells. Journal of immunology *173*, 2428-2434.

HIGHLIGHTS

- Anti-4-1BB IgG2a depletes intratumoral Treg cells but IgG1 promotes CD8 T cells
- The efficacy of anti-4-1BB mIgG1 and mIgG2a depends on different FcγRs
- Optimal tumor therapy requires sequential IgG2a and agonist IgG1 or PD-1 blockade
- Hinge-engineered anti-4-1BB mIgG2a/h2B mAb harnesses both mechanisms of action

IN BRIEF

Buchan et al. reveal dual anti-tumor activities for antibodies to the co-stimulatory receptor 4-1BB, which depend on antibody isotype and FcγR availability. Sequential scheduling of anti-4-1BB and checkpoint blockade mAbs, and antibodies engineered to harness both Treg cell depleting and effector cell agonism properties show potent anti-tumor activity in preclinical models, laying the groundwork for translation into the clinic.

GRAPHICAL ABSTRACT

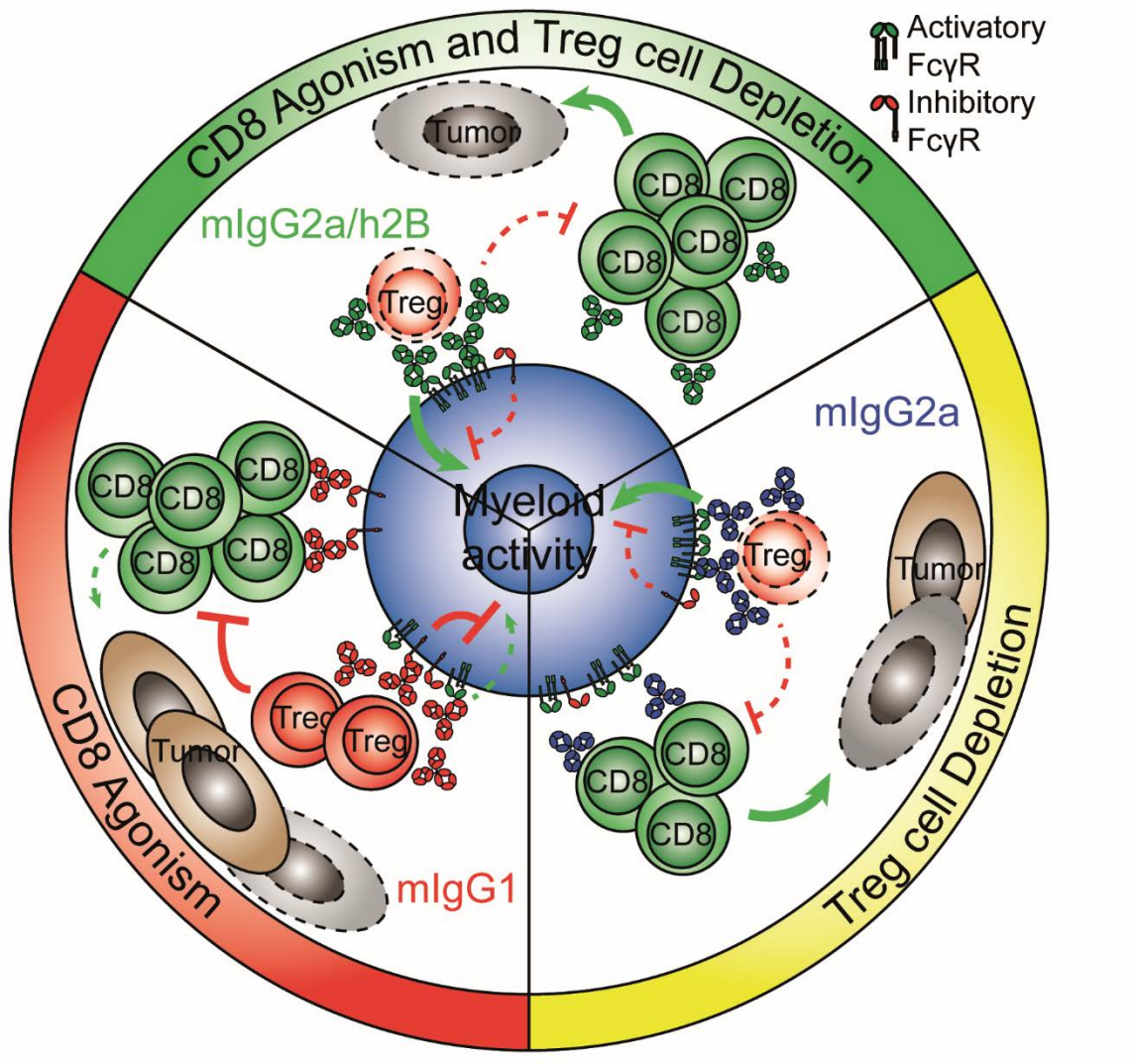

MAIN FIGURE TITLES AND LEGENDS

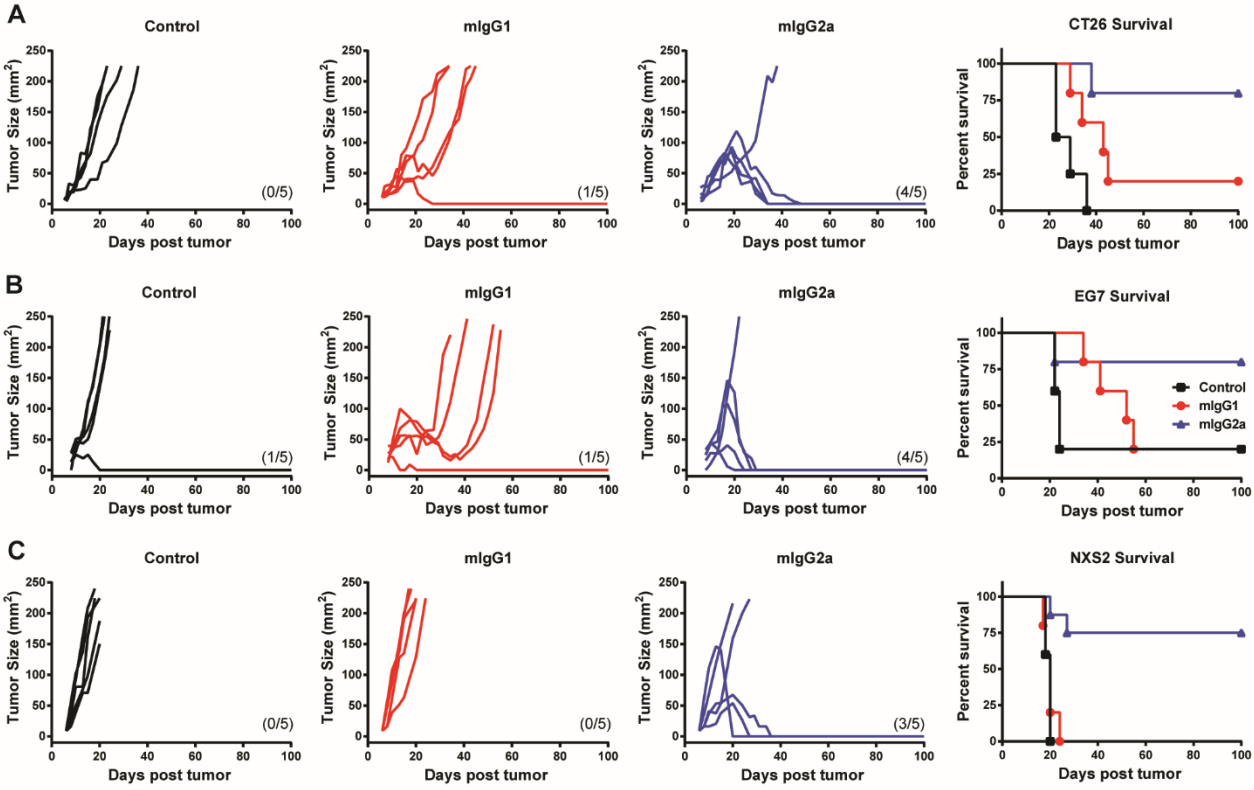

Figure 1.

Figure 1. Anti-4-1BB mIgG2a mAb confers survival benefit in multiple cancer models. (A) Groups of BALB/c mice were challenged with 5 x 10^4 CT26 s.c. on day 0. When tumors were palpable mice received anti-4-1BB (LOB12.0) mIgG1, mIgG2a or PBS control i.v. followed by 3 further administrations i.p. every other day (200 µg final dose). (B) Groups of C57BL/6 mice were challenged with 0.5 x 10^6 EG7 tumour cells s.c. on day 0 prior to 200 µg of anti-4-1BB mAb or PBS control i.p. on days 3, 5 and 7. (C) Groups of A/J mice were challenged with 2 × 10^6 NXS2 cells s.c. and received 200 µg anti-4-1BB mAb or isotype control mAb i.p. when tumor was palpable. A second dose of 200 µg was given 3 days later. In all experimental models tumor growth was monitored and mice culled when mean tumor area exceeded 225 mm^2. Data are expressed as tumor area (mm^2) on the days after tumor challenge as indicated; each line represents an individual mouse. Panels on the right show percentage survival to the humane end-

point. Data represent examples of at least 2 independent experiments where n = 5 mice per group. See also Figure S1 and S2.

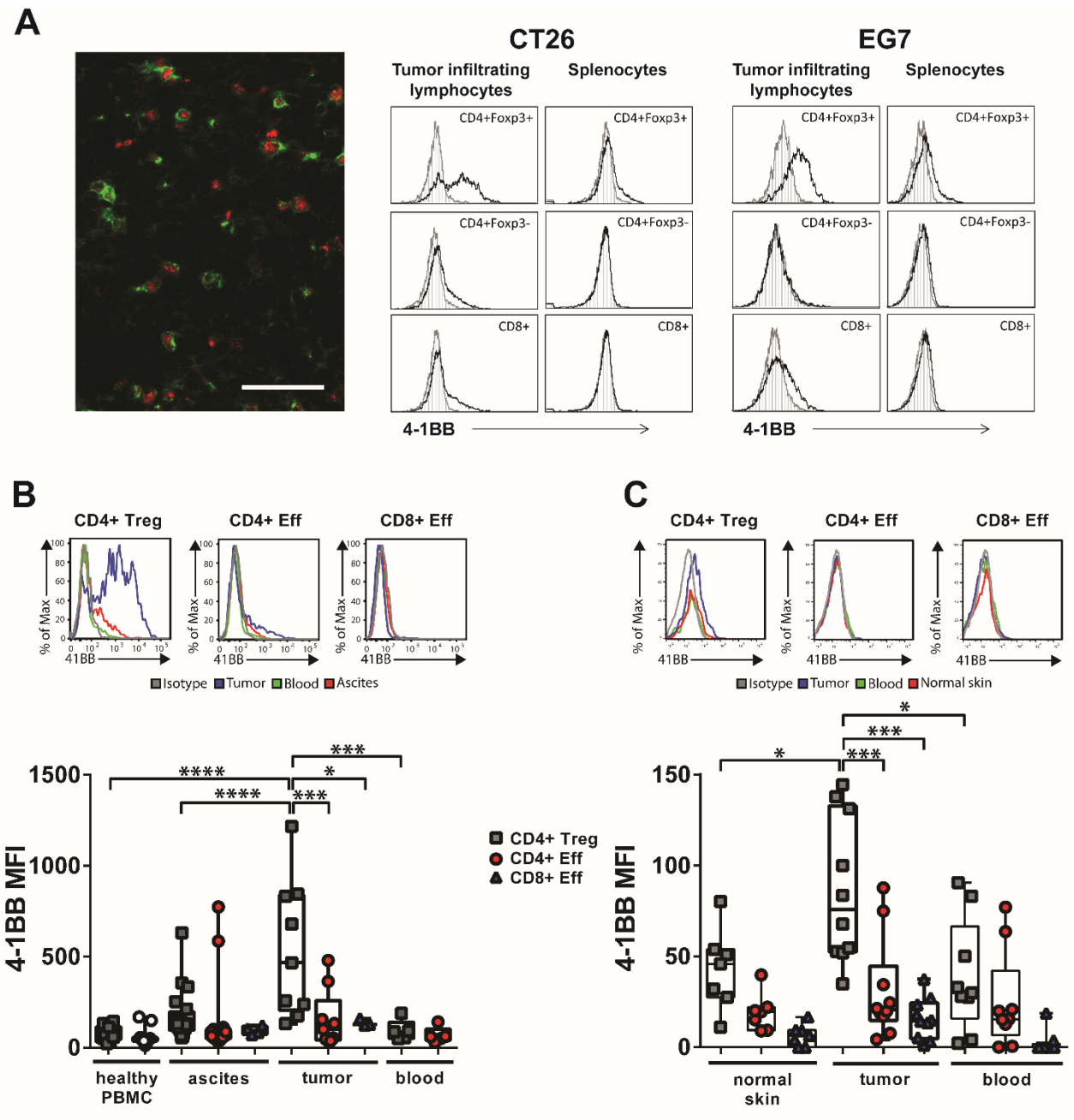

Figure 2.

Figure 2. Mouse and human tumor-resident Treg cells preferentially express 4-1BB. (A; left panel) Immunofluorescence microscopy image showing 4-1BB (green) and Foxp3+ (red) cells in CT26 tumor (left panel). Scale bar = 50 μM. (A; centre and right panels). Flow cytometry histograms demonstrating 4-1BB expression on T-cell subsets from CT26 and EG7 tumor-

infiltrating lymphocytes and splenocytes. 4-1BB expression (black line) on CD4+Foxp3+ (inset top panels), CD4+ Foxp3- (inset middle panels) and CD8+ T cells (inset bottom panels), is shown along with staining with an isotype control antibody (grey line). Representative data for 3 (CT26) or 2 (EG7) experiments are shown, each comprising 3-5 mice. (B) Samples of freshly excised ovarian tumors, ascites and blood were obtained from patients at surgery and compared to healthy PBMC. Tumor samples were minced and digested before separation with a density gradient. Matched peripheral blood was obtained and peripheral blood mononuclear cells were separated by centrifugation. 4-1BB expression was assessed on CD4+CD25+CD127- Treg cells, CD4+ non-Treg cells and CD8+ effector T cells by flow cytometry. Top panels show representative histograms with 4-1BB expression from cells in tumor tissue (blue), blood (green) and ascites (red) from the same patient. Isotype control depicted in grey. Lower panel shows 4-1BB expression on T-cell subsets from different tissue samples. Data points represent individual patients/donors with n = 11 for healthy PBMCs, n = 20 for ascites, n = 9 for tumor and n = 5 for patient blood. (C) Samples of freshly excised cutaneous squamous cell carcinoma (SCC), normal skin and matched blood were obtained from patients at surgery. Samples were minced and digested before separation with a density gradient. Peripheral blood mononuclear cells were separated by centrifugation. Cells were stained for 4-1BB and staining detected by flow cytometry. Top panels show representative histograms with 4-1BB staining shown as open histograms; tumor tissue (blue), blood (green), normal skin (red) and isotype control (grey). Lower panel shows 4-1BB expression on T cell subsets from different tissue samples. Data points represent individual patients/donors with n = 7 for normal skin, n = 10 for tumor and n = 9 for matched patient blood.

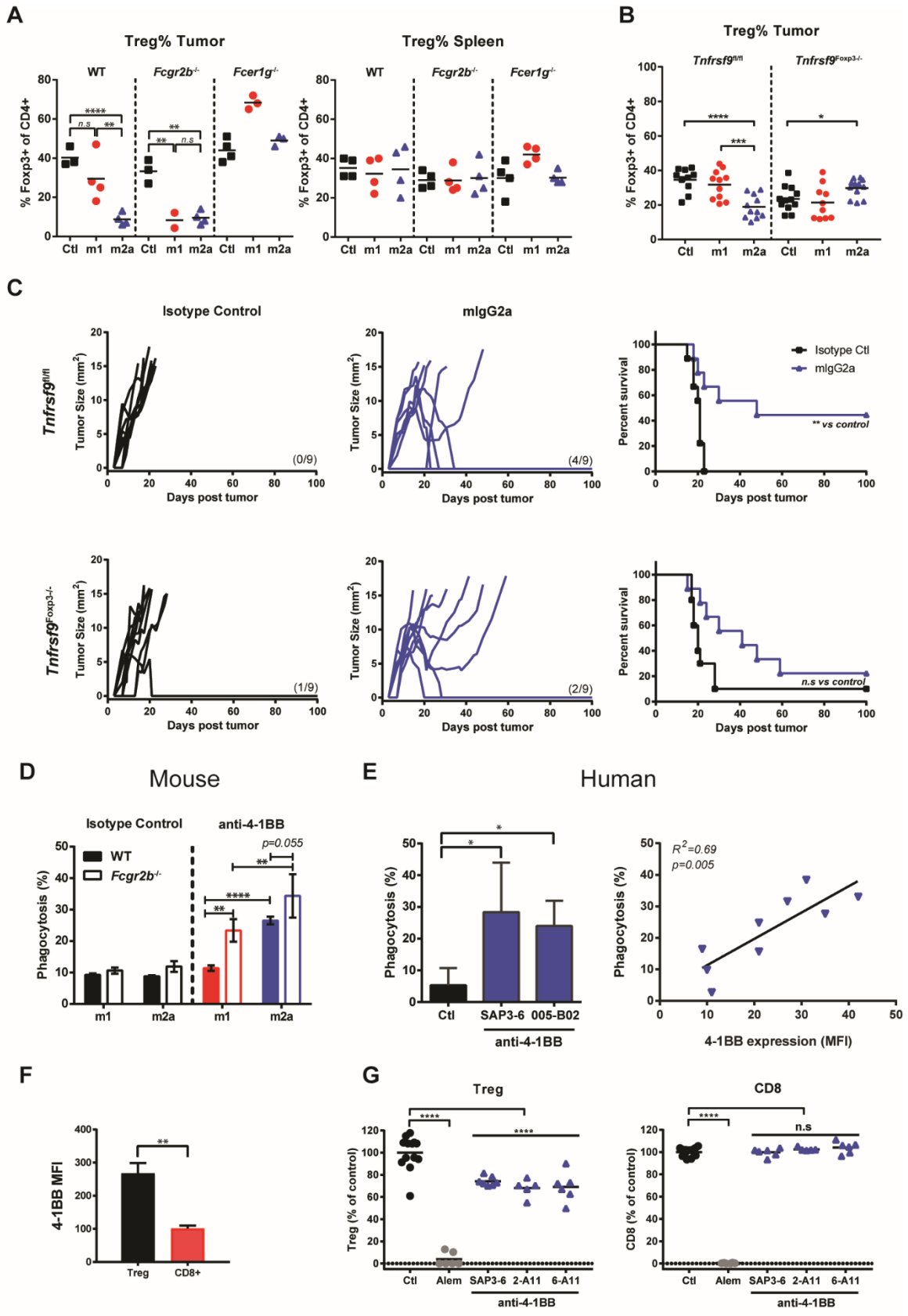
A
Treg% Tumor
Treg% Spleen
WT
Fcgr2b-/-
Fcer1g-/-
% Foxp3+ of CD4+
Ctl m1 m2a
B
Treg% Tumor
Tnfrsf9fl/fl
Tnfrsf9Foxp3-/-
C
Isotype Control
mIgG2a
Tnfrsf9fl/fl
Tnfrsf9Foxp3-/-
Tumor Size (mm2)
Days post tumor
(0/9)
(4/9)
(1/9)
(2/9)
Percent survival
Isotype Ctl
mIgG2a
** vs control
n.s vs control
D
Mouse
Isotype Control
anti-4-1BB
p=0.055
WT
Fcgr2b-/-
Phagocytosis (%)
m1 m2a m1 m2a
E
Human
Phagocytosis (%)
Ctl SAP3-6 005-B02
anti-4-1BB
R2=0.69
p=0.005
4-1BB expression (MFI)
F
4-1BB MFI
Treg CD8+
G
Treg
CD8
Treg (% of control)
CD8 (% of control)
Ctl Alem SAP3-6 2-A11 6-A11
anti-4-1BB
n.s

Figure 3.

Figure 3. Anti-4-1BB mIgG2a mAb mediate Treg cell depletion in solid tumors with activity dependent on both activatory FcγR and 4-1BB expression levels. (A) Groups of 3-4 WT, *Fcgr2b*$^{-/-}$ or *Fcer1g*$^{-/-}$ BALB/c mice received 5 x 10^4 CT26 cells s.c. on day 0. When tumors were palpable mice received anti-4-1BB mIgG1, mIgG2a or PBS control i.v. followed by 3 further administrations i.p. every other day (200 µg final dose). Mice were sacrificed on day 13 and spleen and tumor analyzed by flow cytometry. Data show the frequency of Foxp3+ cells within the CD4+ population in the tumor (left panel) or in matched spleens (right panel). Data are representative of two independent experiments. (B) Groups of *Tnfrsf9*$^{fl/fl}$ or *Tnfrsf9*$^{Foxp3-/-}$ mice received 5 x 10^5 EG7 cells s.c. on day 0 and 200 µg anti-4-1BB mIgG1, mIgG2a or a mix of mIgG1/mIgG2a isotype controls on days 3, 5 and 7. Mice were sacrificed on day 13 and the frequency of Foxp3+ cells out of the CD4+ population in the tumor site determined by flow cytometry. Data points represent individual mice and are pooled from two experiments. (C) Groups of *Tnfrsf9*$^{fl/fl}$ or *Tnfrsf9*$^{Foxp3-/-}$ mice received 5 x 10^5 EG7 cells s.c. on day 0 and 200 µg anti-4-1BB mIgG2a or isotype control mAb i.p. on days 3, 5 and 7. Tumor growth was monitored (left and middle panels; lines represent individual animals) and mice were culled on reaching the humane end point; % survival to the humane end point is shown (right panel). Data are pooled from two experiments (D) CFSE-labelled target murine splenic T cells opsonized with anti-4-1BB mIgG1, mIgG2a or control mAb were co-cultured with wild type (solid bars) or *Fcgr2b*$^{-/-}$ (open bars) mBMDM and then assessed for phagocytosis. Data are from three experiments (E) (left panel) CFSE-labelled target human T cells opsonized with 10 µg/ml anti-human 4-1BB hIgG1 mAb clones SAP3-6, BI005-B02 or control mAb were co-cultured with hMDM and then assessed for phagocytosis, (right hand panel) level of phagocytosis plotted in relation to 4-1BB expression level as determined by flow cytometry. In all cases phagocytosis is

plotted as % of FcγRIIIA/CFSE double positive macrophages. Data are from three independent experiments with mean and SEM from triplicate wells shown. (F) Human PBMCs were injected i.v. into *NOG* mice. After approximately 2 weeks, spleens were taken and expression of 4-1BB on human Treg cells and CD8+ T cells was analyzed by flow cytometry. (G) Splenic cells isolated from *NOG* mice were transferred i.p. into *SCID* mice. 1 hour later, mice were treated i.p. with anti-4-1BB hIgG1, with control mAb or with 10 mg/kg alemtuzumab as a positive control for depletion. Intraperitoneal fluid was collected after 24 hours and frequency of human T cell subsets was determined by flow cytometry. See also Figure S3.

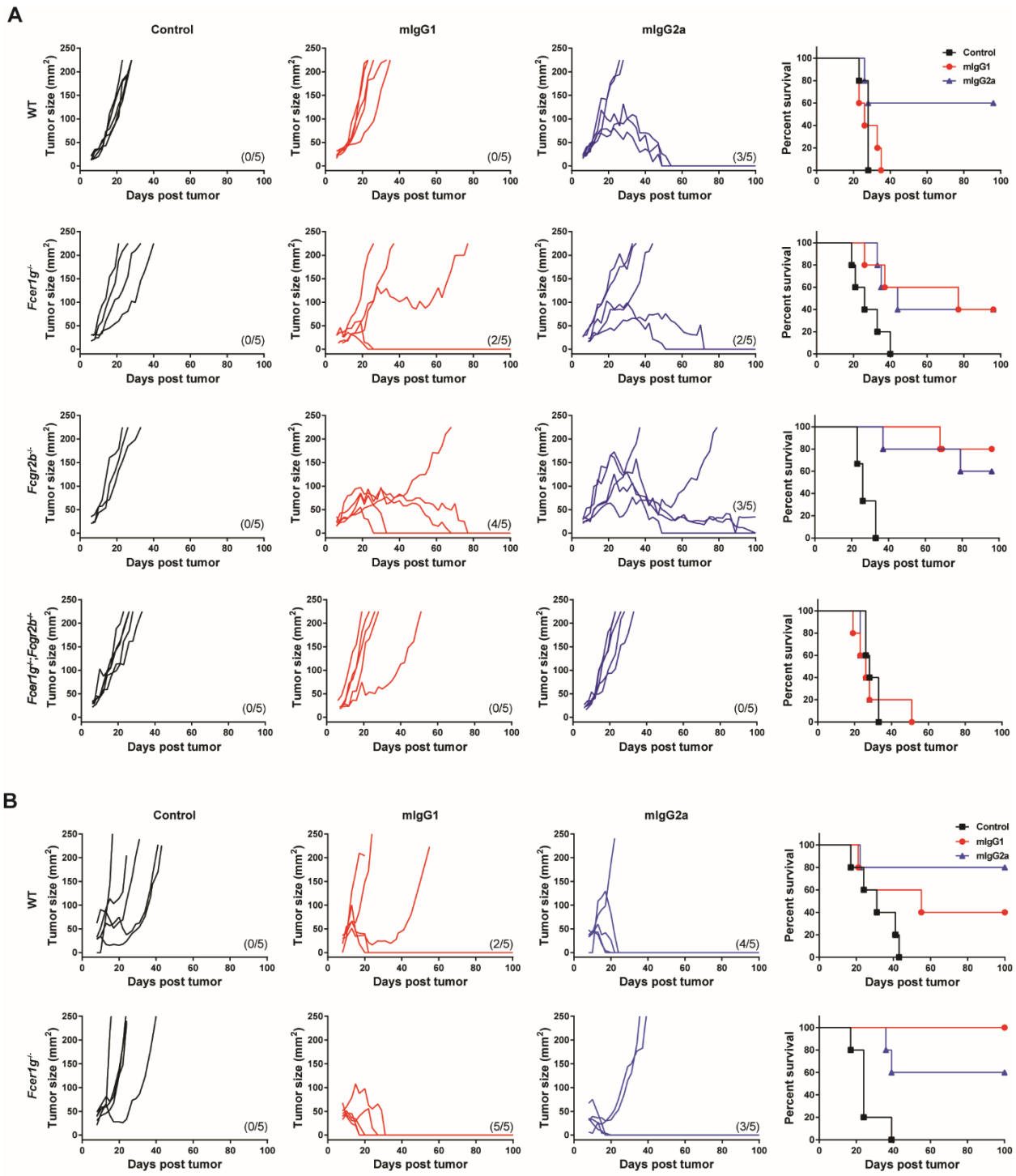

Figure 4.

Figure 4. The primary mechanism of anti-4-1BB mAb therapy in solid tumors is dependent on antibody isotype and FcγR availability. (A) Groups of WT, *Fcer1g*$^{-/-}$, *Fcgr2b*$^{-/-}$ or FcγR null (*Fcer1g*$^{-/-}$;*Fcgr2b*$^{-/-}$), BALB/c mice were challenged with 5 x 10^4 CT26 cells s.c. When

tumors were palpable mice received anti-4-1BB (LOB12.0) mIgG1, mIgG2a or PBS control i.v. followed by 3 further administrations i.p. every other day (200 µg final dose). (B) Groups of WT or *Fcer1g*$^{-/-}$ C57BL/6 mice were challenged on day 0 with 0.5 x 10^6 EG7 tumour cells s.c. On days 3, 5 and 7 mice received anti-4-1BB mIgG1, mIgG2a or PBS control i.p. In both models tumor growth was monitored and mice culled when mean tumor area exceeded 225 mm^2. Data are expressed as tumor area (mm^2) on the days after tumor challenge as indicated; each line represents an individual mouse. Panels on the right show percentage survival to the humane end-point. Data represent examples of at least 2 experiments where n = 5 mice per group.

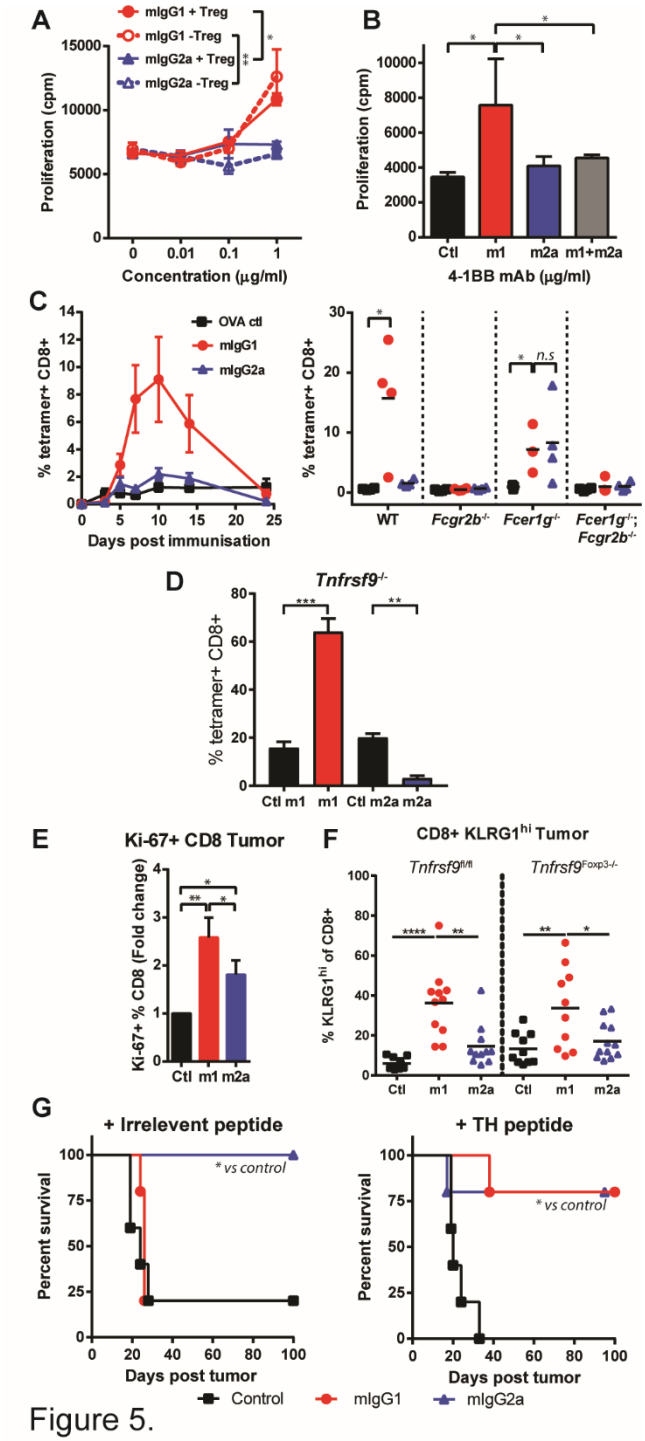

Figure 5.

Figure 5. Anti-4-1BB mIgG1 exerts agonist activity in vitro and in vivo. (A) Splenocytes from mice expressing the *Foxp3-GFP* allele either sorted to remove GFP+ cells (-Treg) or not (+Treg) were incubated with 0.1 µg/ml anti-CD3 and the indicated concentrations of either anti-

4-1BB (LOB12.0) mIgG1 or mIgG2a as indicated. Incorporation of [^{3}H]-thymidine was measured during the last 16 hours of a 72 hour culture. (B) Splenocytes from C57BL/6 mice were similarly incubated with 0.1 μg/ml anti-CD3 and the indicated concentrations of anti-4-1BB mIgG1, mIgG2a or a 1:1 mix of the two prior to assessment of [^{3}H]-thymidine incorporation. Data in (A) and (B) are from individual experiments and show mean (+/-SEM) counts per minute (cpm) of triplicate wells. (C) Groups of mice (wild type; left panel, or the indicated strains; right panel) received 5 mg OVA and 200 μg anti-4-1BB mIgG1 or mIgG2a i.p. on day 0. SIINFEKL-specific CD8 T-cell responses in peripheral blood were quantified by flow cytometry and expressed as a % of total CD8+ cells. Data are from three separate experiments, and show time course of response (mean ± SEM, 6 mice per group) and peak of response (mean and individual responses, 9 mice per group). (D) 1 x 10^5 CD45.1+ purified CD8+ cells from OT-1 mice were adoptively transferred into groups of 3-4 CD45.2+ *Tnfrsf9*$^{-/-}$ recipients. The following day mice were injected with 5 mg OVA and either 200 μg anti-4-1BB mIgG1, anti-4-1BB mIgG2a or with isotype control mAbs. Mice were boosted with mAbs on day 2. Data show the mean (+/-SEM) % CD45.1+CD8+Tetramer+ cells within the total CD8+ population at the peak of the response (day 9) in blood. (E) Groups of 3-4 WT BALB/c mice received 5 x 10^4 CT26 cells s.c. on day 0. When tumors were palpable mice received anti-4-1BB mIgG1, mIgG2a or PBS control i.v. followed by 3 further administrations i.p. every other day (200 μg final dose). Mice were sacrificed on day 13 and tumor analyzed by flow cytometry. Data show the frequency of CD8+, Ki67+ T cells enumerated and plotted as fold change compared to control. Data are representative of two independent experiments. (F) Groups of mice were treated as Fig. 3B and the frequency of Ki-67+ out of the CD8+ population in the tumor site determined on day 13. Data points represent individual mice and are pooled from two experiments. (G) Groups of 5 A/J

mice were challenged with 2×10^6 NXS2 cells s.c. on day 0 and received 200 µg anti-4-1BB mAb or isotype control mAb i.p. and irrelevant (SIINFEKL; left panel) or TH (FETFEAKI; right panel) peptide on day 3. A second dose of mAb (200 µg) was given on day 6. See also Figure S3, S4 and S5.

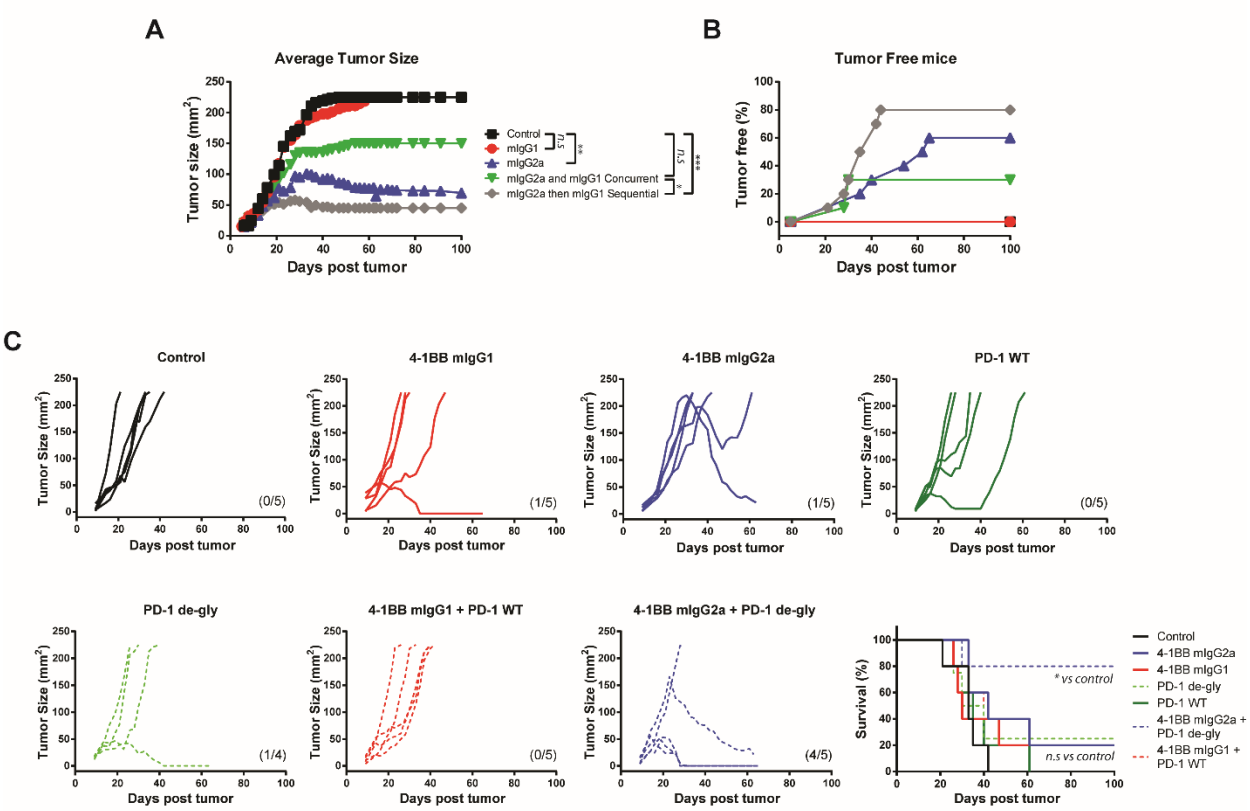

Figure 6.

Figure 6. Anti-4-1BB mIgG2a-mediated Treg cell depletion combines with subsequent anti-4-1BB mIgG1 or anti-PD-1 to enhance tumor therapy. (A and B) Groups of age and sex matched BALB/c mice were challenged with 5 x 10^4 CT26 s.c. on day 0. When tumors were palpable mice received anti-4-1BB (LOB12.0) mIgG1, mIgG2a, concurrent mIgG1 and mIgG2a or PBS control i.v. followed by 3 further administrations i.p. every other day (200 µg final dose). For sequential administration mIgG2a was given i.v. and then mIgG1 given i.p. 4 days later. Tumor growth was monitored and mice culled when mean tumor area exceeded 225 mm^2. In (A) data are expressed as the mean tumor area (mm^2) on the days after tumor challenge as indicated. In (B) data are plotted as percentage of tumor-free mice at specified time points post tumor administration. In A and B data are combined from two independent experiments where n = 10 mice per group. (C) Mice were challenged with CT26 tumor and then given monotherapy as in

(A) or sequential combinations of anti-4-1BB mIgG1 or mIgG2a and/or anti-PD-1 rIgG1 (WT) or its deglycosylated form. For combination treatments anti-4-1BB mAb were administered i.v. when tumors were first palpable and then anti-PD-1 given i.p. 4 days later. Tumor growth was monitored and data plotted to show tumor growth for individual mice and % survival to the humane end-point. Data in (C) represent examples of at least 2 independent experiments where n = 4 or 5 mice per group. See also Figure S6.

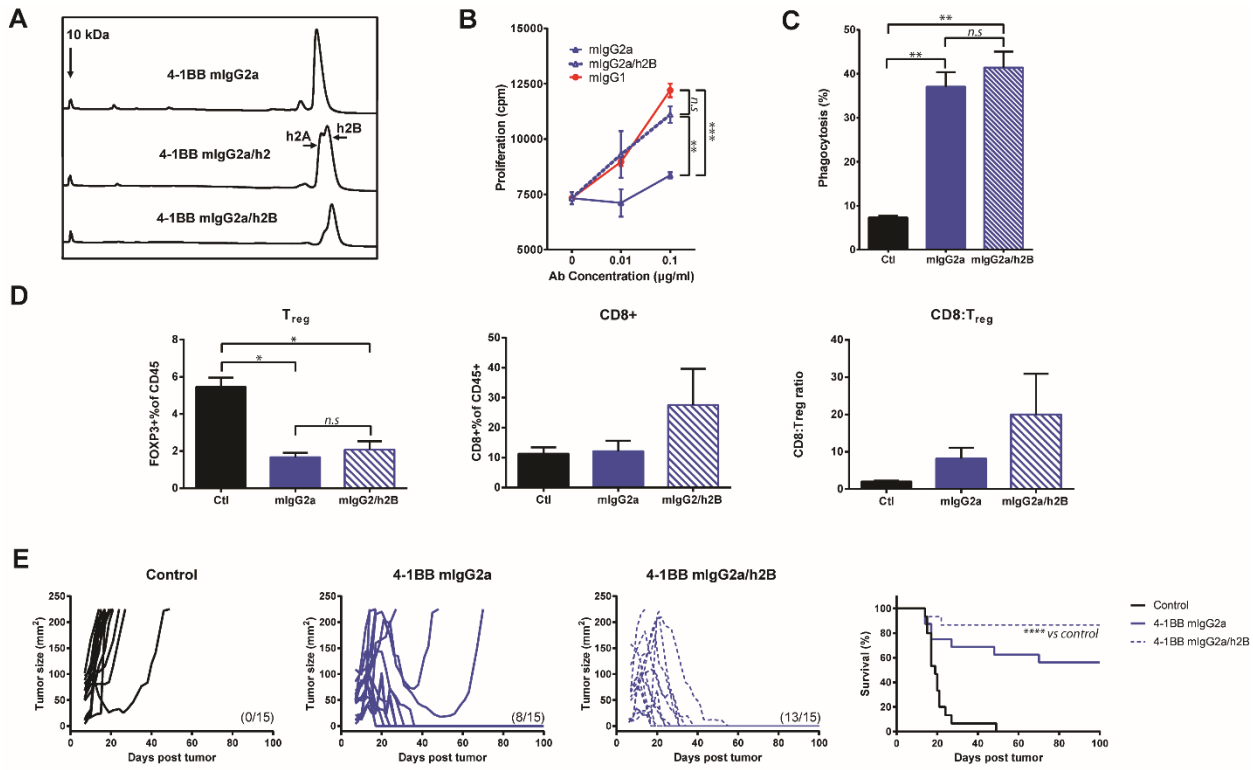

Figure 7.

Figure 7. Fc-engineered anti-4-1BB mIgG2a/h2B possesses dual activity and delivers augmented cancer therapy. (A) Nonreduced capillary electrophoresis-SDS profiles of anti-4-1BB (LOB12.0) mIgG2a, mIgG2a/h2 and 'skewed' mIgG2a/h2B. (B) Splenocytes from C57BL/6 mice were incubated with 0.01 µg/ml anti-CD3 and the indicated concentrations of anti-4-1BB mIgG1, mIgG2a or mIgG2a/h2B as indicated. Incorporation of [^{3}H]-thymidine was measured during the last 16 hours of a 72 hour culture. (C) CFSE-labelled target murine splenic T cells opsonized with anti-4-1BB mIgG2a, mIgG2a/h2B or control mAb were co-cultured with wild type mBMDM and then assessed for phagocytosis. Phagocytosis is plotted as % of double positive (CFSE target cell marker and F4/80 macrophage marker) macrophages. Data in (B) and (C) represent examples of 3 independent experiments where n = 3 per group. (D) Groups of age and sex matched C57BL/6 mice were challenged with 5 x 10^5 EG7 s.c. on day 0. On days 3, 5 and 7 mice received 200 µg mAb or PBS control i.p. as indicated. On day 20 tumors were

harvested and tumor-infiltrating lymphocytes enumerated by flow cytometry. n = 4 mice per group. (E) Mice were set up as in (D), tumor growth was monitored and mice culled when mean tumor area exceeded 225 mm^2. Data represent examples of at least 2 independent experiments where n = 5 mice per group. See also Figure S7.

STAR METHODS

CONTACT FOR REAGENT AND RESOURCE SHARING

Further information and requests for resources should be directed to and will be fulfilled by the lead contact, Stephen Beers (sab@soton.ac.uk).

EXPERIMENTAL MODEL AND SUBJECT DETAILS

Mice

Mice were used in these studies as the least sentient species with an immune system comparable to humans. The availability of transgenic mouse strains also facilitates more detailed understanding of the therapeutic mechanisms used by mAbs to inform clinical translation. C57BL/6, BALB/c, A/J and *Foxp3-GFP* mice were maintained and bred in house. OT-1 TCR transgenic mice (C57BL/6 background) were purchased from Charles River and subsequently bred in house. *Fcer1g*$^{-/-}$, *Fcgr2b*$^{-/-}$ mice were generated by Dr J. Sjef Verbeek, FcγR null (*Fcer1g*$^{-/-}$ x *Fcgr2b*$^{-/-}$) were generated through interbreeding and then brother-sister pairing to generate homozygote FcγR null mice. *Tnfrsf9*$^{-/-}$ mice were generated by backcrossing *Tnfrsf9*$^{tm1a(EUCOMM)Wtsi}$ mice (generated by the International Mouse Phenotyping Consortium and obtained from the Institut Clinique de la Souris, ICS, Strasbourg, France) to C57BL/6 mice and then brother-sister pairing to generate homozygote *Tnfrsf9*$^{-/-}$ mice. *Tnfrsf9*$^{fl/fl}$ mice were generated by crossing *Tnfrsf9*$^{tm1a(EUCOMM)Wtsi}$ mice with a Flp-deleter strain (*B6.129S4-Gt(ROSA)26Sor*$^{tm1(FLP1)Dym}$*/RainJ*; Jackson Laboratory) to excise the FRT-flanked reporter sequence inserted between exons 4 and 5 of *Tnfrsf9* in *Tnfrsf9*$^{tm1a(EUCOMM)Wtsi}$ mice. Mice were then backcrossed to generate *Tnfrsf9*$^{fl/fl}$ mice in which exon 5 of *Tnfrsf9* is flanked by Loxp sites. To generate *Tnfrsf9*$^{Foxp3-/-}$ mice, *Tnfrsf9*$^{fl/fl}$ mice were crossed to *B6.129 (Cg)-Foxp3 tm4*

(YFP/Cre)Ayr/J mice (Jackson Laboratory). Expected mouse genotypes were confirmed by PCR and/or flow cytometry. All mice were bred in a closed research facility under specific pathogen-free conditions. PBMC-*NOG/SCID* mice (primary human xenograft model) were generated by injecting *NOG* mice with 15 x 10^6 PBMC isolated using Ficoll-Paque PLUS in 200ul PBS. *SCID* mice were subsequently injected with 10 x 10^6 splenocytes from reconstituted *NOG* mice. Animal experiments were cleared through local ethical committee and were conducted under U.K. Home Office Project licences PPL30/2964, PB24EEE31 and PA4C79999 and according to H.O. guidelines or at BioInvent under Dnr 14760/2016. Experiments used both male and female mice and mice were age and sex matched within experiments. For the majority of experiments mice were aged between 8-14 weeks. Littermates of the same sex were randomly assigned to experimental groups at the start of the experiment. In some experiments using CT26, mice were grouped after tumour injection but prior to treatment in order to equalise tumour size within groups. For the majority of experiments mice were maintained in SPF conditions in conventional open cages with immunocompromised strains maintained in individually ventilated cages. Food (irradiated RM1 (E)) and water was available *ad libutum*, mice were maintained on a 12 hour light/dark cycle and environmental enrichment was provided; temperature was maintained between 20-24^{o}C. Mice were visually checked daily if adverse effects were anticipated or if mice were nearing a humane end-point.

Human subjects

For in vitro assays using human cells, PBMCs were obtained from anonymised leucocyte cones from the National Blood Service (Southampton U.K.) and used within 4 hours of preparation. Use of human blood samples was approved by local ethical committee. Human PBMCs used in

experiments shown in Figure 3F-H were obtained from Hallands hospital Halmstad, Sweden. For clinical samples, ethical approval was obtained from Southampton University Hospital NHS Trust, Southampton and South West Hampshire Research Ethics Committee or by the Ethics Committee of Skåne University Hospital, Sweden. Clinical samples were released from the Human Tissue Authority licensed University of Southampton, Cancer Sciences Unit Tissue Bank, obtained through the Department of Obstetrics and Gynecology and the Department of Oncology at Skånes University Hospital, Lund, Sweden, or obtained from patients undergoing surgery at the Dermatology Department, University Southampton Hospital NHS Foundation Trust as approved by the South Central Hampshire B National Research Ethics Service Committee (Reference number 07/H0504/187). Informed consent for the use of human material was provided in accordance with the Declaration of Helsinki.

Cell lines

The CT26 colon carcinoma (Taraban et al., 2002), NXS neuroblastoma (Lode et al., 1997), B16/BL6 melanoma, B16-sFlt3L-Ig (FVAX: (Curran and Allison, 2009)), EG7 (Moore et al., 1988) and Karpas-299 anaplastic large cell lymphoma stably transduced with a tail-less form of murine 4-1BB (pTL; (Buchan and Al-Shamkhani, 2012) have all been described previously. Cells were maintained in a humidified incubator at 37^{o}C and 5% CO_2 in Dulbecco's modified eagles medium (DMEM; EG7, B16/BL6 and FVAX) or RPMI-1640 (CT26, Karpas-299) supplemented with 10% heat inactivated FCS, 2mM L-glutamine, 1mM pyruvate, 100U/ml penicillin and 100µg/ml streptomycin. EG7 cells were additionally cultured in the presence of 0.4mg/ml geneticin which was removed one day prior to injection. NXS2 cells were maintained in DMEM supplemented with 10%FCS, 2mM L-glutamine and 0.1mM nonessential amino

acids. All cells were cultured for a maximum of 3 months before returning to a frozen stock in order to prevent drift. Cell lines are routinely tested for mycoplasma in house. Prior to injection, cells were visualised under a microscope to ensure viability and verify that they exhibited the expected phenotype. The identity of Karpas-299 cells was verified previously by the surface expression of CD30 and expression of an ALK rearrangement (Buchan and Al-Shamkhani, 2012). As expected melanoma cell lines appeared black in culture as a consequence of melanin expression.

METHOD DETAILS

Antibodies and reagents

Anti-4-1BB (clone LOB12.0) mAb mIgG1, mIgG2a and mIgG2/huIgG2 CH1 hinge (mIgG2a/h2B) isotypes were constructed as previously described (White et al., 2011; White et al., 2015). Anti-CD8 (clone YTS169) was produced in house. Anti-mouse PD-1 (EW1-9) mAb rIgG1 was raised using conventional hybridoma technology after immunisation of Wistar rats with recombinant mouse PD-1 (Leu25-Gln167) Fc fusion protein (R&D Systems). Spleen from immunised rats or mice were fused with NS-1 myeloma cells and plates screened by ELISA and flow cytometry. mAbs were initially screened and cells in positive wells were cloned twice and expanded in culture for IgG production. Antibodies were produced from hybridoma or CHOK1 cells and purified on Protein A with purity assessed by electrophoresis (Beckman EP system; Beckman Coulter, Buckinghamshire, U.K.) and lack of aggregation by SEC HPLC (all mAb less than 1%). All preparations were endotoxin low (<10 EU endotoxin/mg) as determined using the Endosafe-PTS portable test system (Charles River Laboratories, L'Arbresle, FR). Anti-PD-1 de-gly was produced by treating EW1-9 with 0.05 U of PNGaseF/μg of antibody. N-Glycosidase F (PNGaseF) was obtained from Promega (V483A). Samples were kept at 37^{o}C overnight. De-glycosylation was confirmed either by electrophoresis or SPR analysis. Purification of antibody from enzyme was achieved through size exclusion chromatography using sephadex^{TM}200. % Aggregation was less than 1% for all mAbs. Peptides were either produced in house (SIINFEKL) or obtained from Peptide Protein Research Ltd (SIINFEKL, FETFEAKI). Other reagents are detailed in the Key Resources Table. PE-labelled SIINFEKL peptide/H-2K^{b} tetramer was manufactured in house (Protein Core Facility, University of Southampton).

Surface Plasmon Resonance

Analyses of anti-41BB mAb interactions with soluble FcγR were assayed using a Biacore T100 (GE Healthcare Life Sciences, Buckinghamshire, UK). Antibodies or BSA as a control were immobilized at 5000 resonance units [RU]) to the flow cells of CM5 sensor chips (GE Healthcare Life Sciences, Buckinghamshire, UK) by standard amine coupling according to the manufacturer's instructions. Soluble FcγR (R&D Systems, Abingdon, U.K.) were injected through the flow cells at 1500, 375, 94, 23, 6, and 0 nM in HBS-EP+ running buffer (GE Healthcare Life Sciences, Buckinghamshire, UK) at a flow rate of 30µl/min. Soluble Fc receptor was injected for 2 min, and dissociation was monitored for 5 min. Background binding to the control flow cell was subtracted automatically. Affinity constants were derived from the data by equilibrium binding analysis as indicated using Biacore Bioevaluation software (GE Healthcare Life Sciences, Buckinghamshire, UK). To determine the binding of anti-PD-1 mAbs to FcγRs, an anti-histidine mAb (GE Healthcare) was used to capture FcγRI, IIB, III or IV onto a CM5 chip before soluble mAbs were passed on top. To demonstrate that anti-PD-1 mAb blocks PD-L1 binding to PD-1, recombinant PD-1-his (R&D Systems) was similarly captured on a CM5 chip with an anti-histidine mAb before passing over PD-L1-Fc (R&D Systems) or anti-PD-1 mAbs as indicated.

In vitro binding assays

Karpas-299 cells stably transduced with a tail-less form of murine 4-1BB (pTL) were incubated with the concentrations of anti-4-1BB mAb indicated at 4^{o}C for 20 mins prior to washing and staining with a PE-labelled anti-mouse or anti-rat secondary antibody (Jackson Immunoresearch). No staining was observed to Karpas-299 cells stably expressing an empty

vector control (data not shown). For the competitive binding assay, 0.1 μg/ml parental rat anti-4-1BB mAb was mixed with graded concentrations of either mIgG1 or mIgG2a versions of anti-4-1BB as indicated prior to incubation with Karpas-299 pTL cells. Cells were washed and stained with an APC-conjugated and mouse-adsorbed donkey anti-rat secondary antibody; the secondary antibody did not bind to either mIgG1 or mIgG2a (data not shown). Flow cytometric analysis was performed using a BD FACS Canto II and FACS Diva software.

Immunotherapy protocols

CT26 - Groups of age and sex matched WT, *Fcer1g*$^{-/-}$, *Fcgr2b*$^{-/-}$ or FcγR null (*Fcer1g*$^{-/-}$;*Fcgr2b*$^{-/-}$) BALB/c mice were challenged with 5 x 10^4 CT26 cells s.c. on day 0. When tumors were palpable mice received mAb or PBS control i.v. followed by 3 further injections i.p. every other day (200 μg final dose unless otherwise indicated). Where CD8+ T cells were depleted, 0.5 mg of anti-CD8 (YTS169) was administered i.p. on days -1, +1, and +4 as previously described (French et al., 1999) relative to administration of tumor. For rechallenge experiments mice surviving the initial tumour challenge and naïve control mice were rechallenged after day 100 with 5x10^4 CT26 cells s.c. and monitored for tumour growth.

EG7 – Groups of age and sex matched C57BL/6, *Tnfrsf9*$^{fl/fl}$, *Tnfrsf9*$^{Foxp3-/-}$ or *Fcer1g*$^{-/-}$ C57BL/6 mice were challenged with 5x10^5 EG7 cells s.c. on day 0 prior to injection of 200 μg mAb, 200 μg isotype control mAb or PBS control as indicated on days 3, 5 and 7 i.p.

NXS2 – Groups of age and sex matched A/J mice were challenged with 2x10^6 NXS2 cells s.c. on day 0 and received antibody/peptide vaccine as specified in individual experiments. All antibodies were given i.p. in PBS. Tyrosine Hydroxylase (FETFEAKI) and control (SIINFEKL)

peptides in PBS were emulsified in equal volumes of incomplete Freunds adjuvant (IFA) before injection i.d.

B16/BL6 - Groups of age and sex matched C57BL/6 mice were challenged with 2.5 x 10^4 B16/BL6 cells intra-dermally on day 0. On days 3, 6 and 9 mice received 1 x 10^6 irradiated FVAX cells i.d. on the opposite flank and either PBS, 100 µg anti-CTLA-4 (clone 9D9) or anti-CTLA-4 and 300 µg anti-4-1BB antibodies as indicated i.p. also on day 3, 6 and 9 based on our previously published protocol (Curran et al., 2011).

In all models, tumour growth was regularly monitored by caliper and mice culled when cross-sectional area exceeded 225 mm^2.

In vitro cell proliferation

Spleens from *Foxp3-GFP* mice were sorted on a FACsAria to exclude GFP+ cells (-Tregs; 99% of Treg cells removed; data not shown) or null sorted and plated at 1 x 10^5 cells/well with 0.1µg/ml anti-CD3 (145.2C11) and a range of anti-4-1BB mAb concentrations as indicated. 1 µCi/well [3H]-thymidine was added 56 hours later and plates harvested after a further 16 hours culture.

To determine if anti-4-1BB mIgG1 and mIgG2a induce dilution of CFSE by murine T cells in vitro, splenocytes from C57BL/6 mice were labelled with CFSE (5x10^7 cells/ml in 10µM CFSE for 5 mins) and cultured for 72 hours with soluble anti-CD3 (clone 145.2C11) at the concentrations shown and with 10 µg/ml anti-4-1BB mIgG1, mIgG2a or with an equal mix of mIgG1 and mIgG2a isotype control mAbs. Cells were then stained for CD8 and the CFSE content of cells visualised on a FACsCanto II.

Endogenous OVA-specific immune responses

Mice were immunized on day 0 with 5 mg OVA (Sigma) and 200 μg mAb i.p. The expansion of endogenous OVA-specific CD8+ T cells in peripheral blood was monitored over time and analyzed by flow cytometry as described previously (White et al., 2011).

Expansion of transferred OT-1 cells

Splenocytes from OT1 transgenic mice were harvested, washed and approximately $2x10^5$ OVA-specific CD8+ T cells were then transferred into recipient C57BL/6 mice by tail vein injection. The following day mice were immunised with 0.5 mg OVA alone or delivered with 200 μg anti-4-1BB mIgG1 or mIgG2a mAbs. Expansion of OT1 T cells in peripheral blood was analysed by flow cytometry as previously described (White et al., 2011). To determine expansion of adoptively transferred OT-1 T cells in recipient mice lacking 4-1BB expression, $1x10^5$ purified CD8+ T cells (CD8 positive selection MACs, Miltenyi Biotech) from CD45.1+OT-1 mice were adoptively transferred to *Tnfrsf9*$^{-/-}$ or *Tnfrsf9*$^{Foxp3-/-}$ mice on day 0. The following day mice were injected with 5 mg OVA and 200 μg anti-4-1BB mIgG1 or mIgG2a or with OVA and isotype control mAbs i.p. Mice received another boost of mAb i.p. on day 2. Expansion of adoptively transferred cells in the peripheral blood was carried out on the days indicated by staining for CD45.1, CD8 and with a PE-labelled H-$2K^b$/SIINFEKL tetramer (in house).

Lymphocyte isolation

Mouse tissue - In some experiments mice challenged with CT26 or EG7 had their tumors excised and digested with 0.5 WU/ml Liberase DL (Roche) and 50 μg/ml DNaseI (Roche) for 20-45

mins at 37ºC. Cells were then passed through a 100 μm cell strainer and used for assays directly or tumor infiltrating lymphocytes were isolated using percoll gradients of 40% and 70%.

Human tissue - Ascitic fluid was assessed directly as a single cell suspension. Ovarian tumor samples were cut into small pieces and incubated in supplemented RPMI1640 with DNase I (Sigma) and Liberase TM (Roche Diagnostics) for 20 min at 37°C. Remaining tissue was mechanically dissociated and, together with the cell suspension, passed through a 70 μm cell strainer. Samples of freshly excised cutaneous squamous cell carcinoma (cSCC) and normal skin were minced and treated with 1mg/ml collagenase IA (Sigma) and 10 μg/ml DNAse I (Sigma) in RPMI medium (Gibco) at 37°C for 1.5 hours before straining through a 70 μm cell filter (BD) and centrifugation (600 x *g*, 20 minutes) over an Optiprep (Axis-Shield) density gradient. Matched peripheral blood samples were obtained and peripheral blood mononuclear cells were separated by centrifugation over Lymphoprep (Axis-Shield) at 600 x *g* for 30 minutes.

Flow cytometry of murine cells

For the detection of CD8+ T cell expansion in the blood, lymphocytes were washed and incubated with 10 μg/ml 2.4G2 FcR block for 15 minutes at 4^0C. Fluorochrome-labelled antibodies to surface markers were then added for 20-30 minutes in PBS + 1% BSA and the cells washed once with PBS/1% BSA. Red blood cells were lysed with either ammonium chloride buffer (in house) or with Erythrolyse Red Blood cell lysis buffer (AbD SeroTec) and samples washed once with PBS/1% BSA. Samples were then run on a BD FACSCanto II or FACSCalibur and data analyzed using FCS Express or FACs Diva software. Staining of lymphocytes from spleen and tumours was performed similarly. In some cases, tumour samples were additionally stained with a fixable live/dead stain (eBioscience) to visualise only the live

cell population. For intracellular staining, cells were surface stained and then fixed and intracellularly stained using the anti-Mouse/Rat Foxp3 Staining Set (BD Biosciences). Antibodies were anti-CD4 eF450 (GK1.5), anti-CD8-APC-eF780 or -FITC (53-6.7), anti-Foxp3 APC or -PE (FJK-16), anti-4-1BB-PE or -eF450 (17-B5), anti-KLRG-1-APC (2F1), anti-MHCII-APC-eF780 (M5/114.15.2), anti-CD11c-APC (N418), streptavidin-PE-Cy7 (all eBioscience), anti-Ki67 APC (B56) (BD Biosciences), anti-4-1BB-biotin (Biolegend) or isotype controls.

Flow cytometry of human cells

Before staining with relevant antibodies, cells from ovarian cancer patients were incubated for 10 mins with 10mg/ml KIOVIG (Baxalta). Cells were stained with either fixable eFluor780 Live/Dead stain (eBioscience) or aqua live/dead viability stain (Invitrogen) at 4°C in PBS. For cell surface staining antibodies were incubated with cells in the dark for 30 minutes at 4°C in PBS/1% BSA + 10% FCS (Gibco). Intracellular staining was with a Foxp3 staining buffer set (eBioscience). Cells were analyzed by flow cytometry using a BD FACSAria or BD FACSVerse. Fluorophore conjugated antibodies against the following cell markers were used: Ovarian samples - CD4-BV510 (RPA-T4), CD25-BV421 (M-A251), CD127-FITC (HIL-7R-M21), CD8-APC (RPA-T8), 41BB-PE (4B4-1), mouse IgG2a isotype,κ control-PE (G155-178; all from BD Biosciences); SCC- CD3-APC-Cy7, CD4-FITC or PerCP Cy5.5, CD8-PE Cy7 (all Biolegend), 4-1BB-PE and Foxp3-APC (both eBioscience).

Immunofluorescence

Tumour tissue was embedded in OCT (CellPath) and frozen in isopentane on dry ice. 8 μm frozen sections were fixed in acetone and incubated sequentially with; rat anti-mouse 41BB (in house), Alexa Fluor 488-conjugated goat anti-rat IgG (Life Technologies), rabbit anti-mouse FoxP3 (Abcam) and Alexa Fluor 568-conjugated goat anti-rabbit IgG (Life Technologies). Nuclei were counterstained with DAPI (Life Technologies) and mounted in Vectashield (Vector Laboratories). Images were collected using a CKX41 inverted microscope reflected fluorescence system equipped with a CC12 colour camera running under Cell B software (Olympus, UK).

Antibody-dependent cellular phagocytosis

ADCP assays were performed as described previously with mouse (Beers et al., 2008; Beers et al., 2010) or human macrophages (Lim et al., 2011; White et al., 2011). Briefly, bone marrow derived macrophages (BMDM) were generated from the femurs of C57BL/6 or *Fcgr2b*$^{-/-}$ mice and cultured in complete RPMI containing 20% L929 supernatant. Alternatively, human monocyte derived macrophages (hMDMs) were generated from PBMCs and cultured in complete RPMI containing M-CSF (in house). Mouse 4-1BB-expressing target cells were generated by isolating splenocytes from WT mice and stimulating in vitro with soluble anti-CD3 (48 hours, 1 μg/ml clone 145.2C11). Human target cells were generated from CD4+ cells isolated from PBMC using negative selection with Human CD4+ T cell isolation kit (EasySep). To increase 4-1BB expression cells were plated at $1.5x10^6$ cells/ml and treated overnight with 0.01, 0.1 or 1 mM DMOG (Sigma); expression of 4-1BB was then assessed by flow cytometry (data not shown). Target cells were subsequently CFSE-stained (5 μM) then opsonized with the anti-4-1BB mAbs indicated before being co-cultured with macrophages for 1 hour. Cell mixtures

were stained with anti-CD16-APC (human) or anti-F4/80-APC (mouse) and samples assessed for the percentage of double positive (CFSE/APC) macrophages by flow cytometry.

Assessment of Treg cell depletion in reconstituted NOG/SCID mice

Approximately two weeks after reconstitution of *NOG* mice with human PBMCs, spleens were isolated and rendered into a single cell suspension. Thereafter, a small sample was taken to determine the expression of 4-1BB on human T cells by flow cytometry. To examine Treg cell depletion, *SCID* mice were injected with 10×10^6 splenocytes from reconstituted *NOG* mice 1 hour prior to injection with 10 mg/kg alemtuzumab or isotype control mAb. The intraperitoneal fluid of mice was collected after 24 hours and human T-cell subsets were identified and quantified by flow cytometry using the following markers: CD45, CD4, CD8, CD25 and CD127.

QUANTIFICATION AND STATISTICAL ANALYSIS

Data analysis throughout was performed using GraphPad Prism 6.0 for Windows software. Where averages and error bars are indicated these are means and standard error of the mean. Individual data points for in vivo experiments refer to one individual mouse. Similarly for the human data shown in Figure 2, individual points represent patients/donors. Statistical analyses of pair-wise comparisons are by two-tailed, non-paired Students t-test and for multiple comparisons by one-way or two-way ANOVA with Tukey's post-hoc multiple comparisons test, as appropriate. $p<0.05$ is considered significant throughout. N numbers are defined in the relevant legends. Group sizes for murine experiments were determined by previous experience with similar models which indicate that 5 mice/group is usually sufficient to obtain statistical significance. Statistical comparisons between survival to the humane end point are by Log-rank

test, and again statistical significance is considered at $p<0.05$. Throughout *$p<0.05$, **$p<0.01$, ***$p<0.001$, ***$p<0.0001$. Analysis in Figure 3E was by Pearson's correlation coefficient; $p<0.05$ is considered significant.

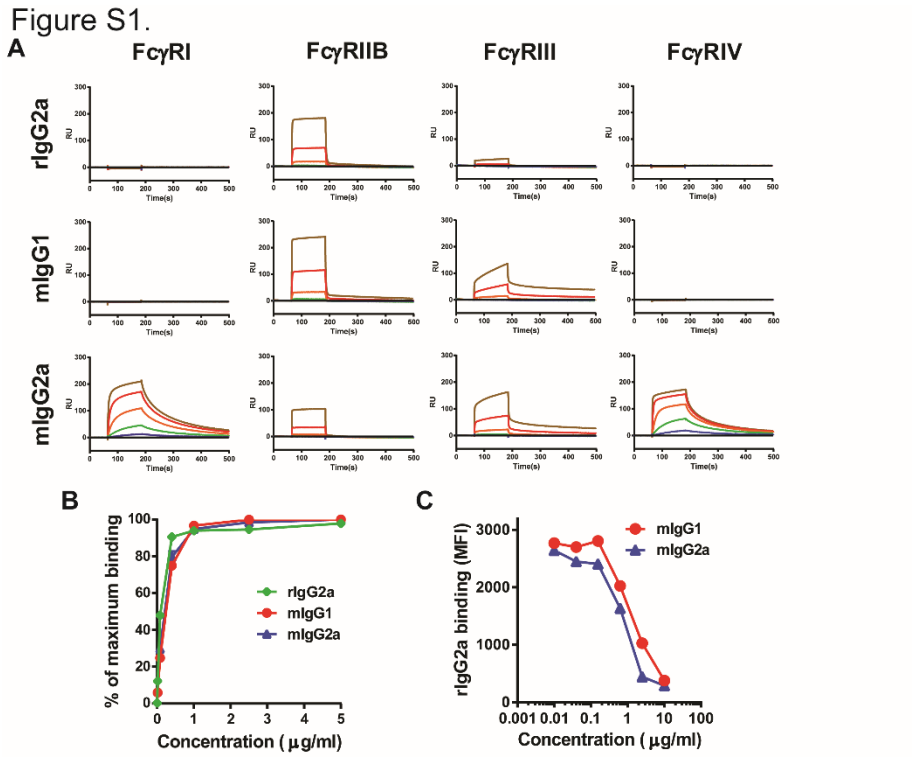

Figure S1, related to Figure 1. Anti-4-1BB mAb characterization. (A) Surface plasmon resonance analysis of anti-4-1BB (clone LOB12.0) mIgG1, mIgG2a and the parental rIgG2a binding to mouse FcγRI, IIB, III and IV. Recombinant, soluble FcγR protein (0 - black, 6 - blue, 23 - green, 94 - orange, 375 - red, 1500 nM - brown) was passed over anti-4-1BB mAb immobilized at 5000 RU. Sensorgrams are shown. (B) A human cell line stably transfected with a construct encoding the extracellular and transmembrane region of murine 4-1BB was incubated with anti-4-1BB of mIgG1, mIgG2a isotype or with the parental rIgG2a mAb at a range of concentrations prior to staining with a PE-labelled secondary antibody. Data show mean fluorescence intensity at each concentration as a percentage of maximum. (C) Rat anti-4-1BB was mixed with mouse mIgG1 or mIgG2a anti-4-1BB mAb at the concentrations indicated, prior to incubation with a murine 4-1BB transfected cell line. Rat mAb binding was detected with an anti-rat secondary antibody and data are expressed as mean fluorescence intensity of the rat anti-4-1BB antibody relative to the concentration of competitive mouse anti-4-1BB.

Figure S2.

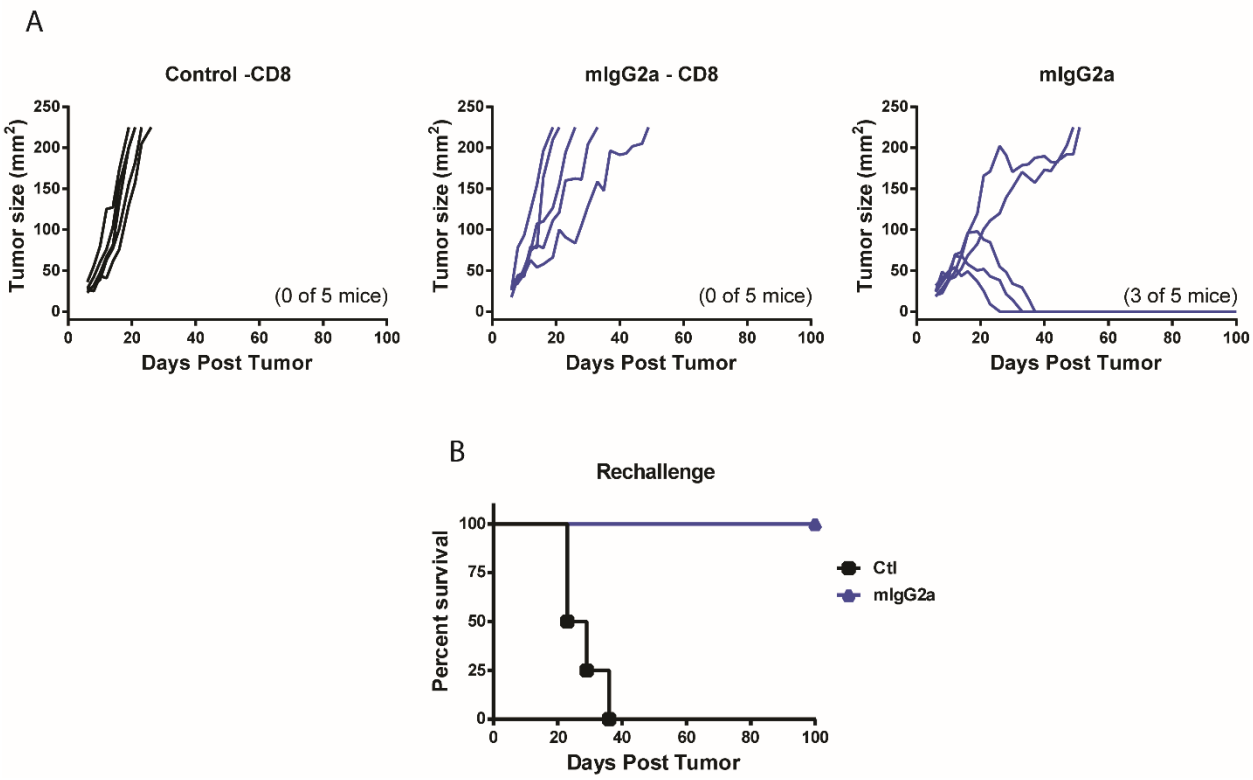

Figure S2, related to Figure 1. Anti-tumor efficacy of anti-4-1BB mIgG2a mAb is dependent upon CD8+ T cells and provides long term anti-tumor protection. (A) Groups of BALB/c mice were treated, or not, with 500 µg of a CD8-depleting antibody on days -1, 1 and 4 relative to challenge with 5 x 10^4 CT26 cells s.c. on day 0. Anti-4-1BB mIgG2a mAb was administered on day 6 i.v., and on days 8, 10 and 12 i.p., to a final total dose of 200 µg. Tumor sizes were recorded and mice culled when mean tumor diameter reached 15 mm. Data show tumor area (mm^2) on the days indicated after tumor challenge with each line representing an individual mouse. (n = 5/group) (B) Long term (100 days) surviving anti-4-1BB mIgG2a treated CT26 mice and naive controls were rechallenged with CT26 as in (A) and survival to humane end-point plotted. (n = 4-5/group).

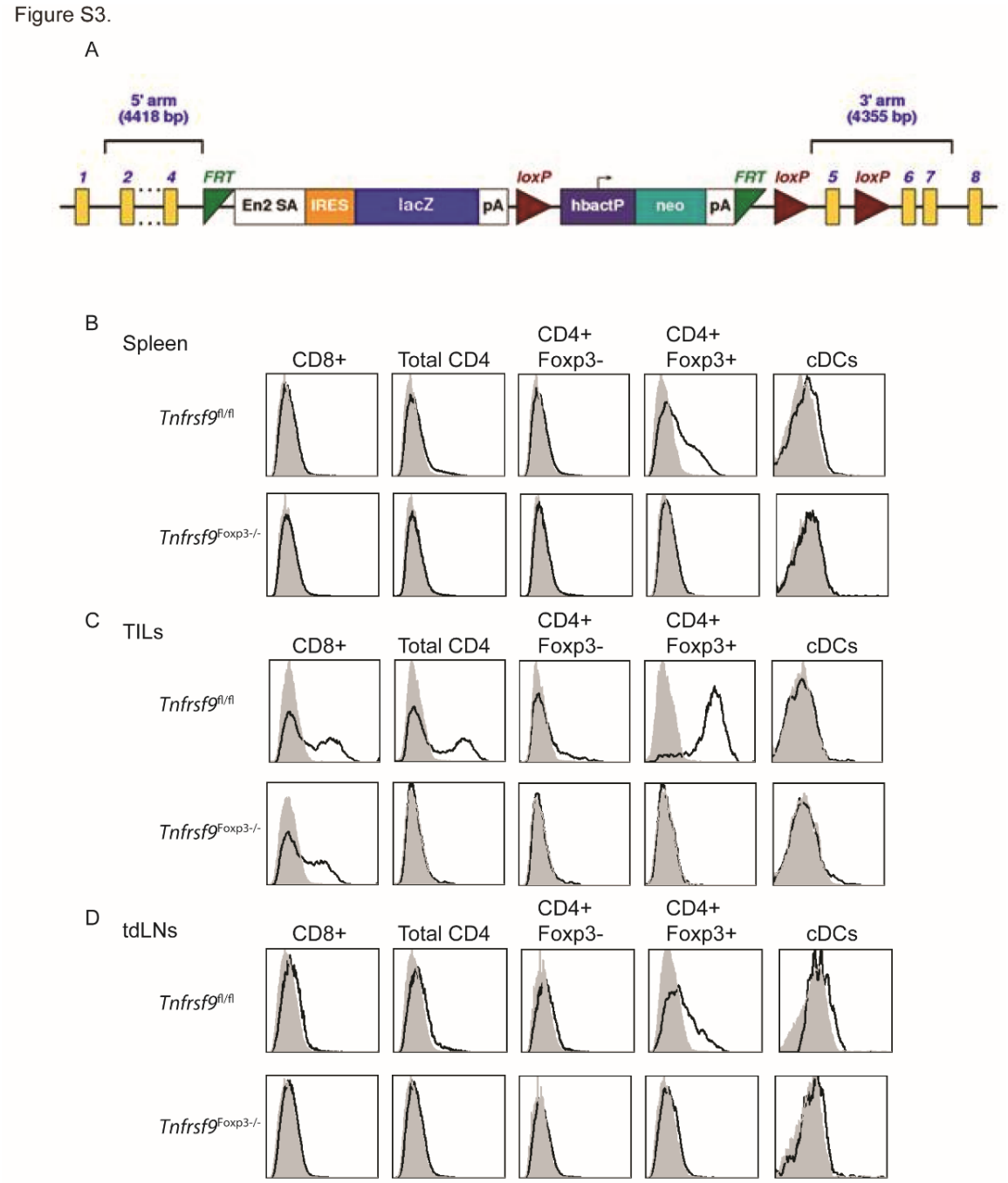

Figure S3, related to Figures 3 and 5. Schematic of 4-1BB targeting strategy for generation of *Tnfrsf9*$^{-/-}$ and *Tnfrsf9*$^{Foxp3-/-}$ mice and 4-1BB expression data in *Tnfrsf9*$^{Foxp3-/-}$ mice. (A) Schematic of the targeted 4-1BB locus in *Tnfrsf9tm1a(EUCOMM)Wtsi* strain (courtesy of the European Conditional Mouse Mutagenesis (EUCOMM) Program)**.** *FRT*, flippase recognition target; *En2 SA*, Engrailed-2 splice acceptor; *IRES*, internal ribosomal entry site; *lacZ*, lactose

operon whose gene product is β-galactosidase; *pA*, polyadenylation tail; *loxP*, locus of X-over P1; *hBactP*, human β-actin promoter5; *neo*, neomycin. (B-D) 0.5 x 10^6 EG7 tumour cells were injected into groups of 5 age-matched *Tnfrsf9*$^{fl/fl}$ or *Tnfrsf9*$^{Foxp3\text{-}/\text{-}}$ mice s.c. on day 0. Mice were culled on day 17 and (B) spleen, (C) tumor and (D) tumor-draining lymph nodes (bilateral iLNs) were dissected, processed, stained and analyzed by flow cytometry. Tumors were digested with Liberase DL/DNase I as detailed in the Methods. Isolated cells were stained with anti-CD8-FITC, anti-CD4-eFluor450, anti-Foxp3-PE, anti-MHCII-APC-Cy7, anti-CD11c-APC and anti-4-1BB-biotin followed by streptavidin-PE-Cy7. Tumor samples were additionally stained with fixable viability dye eF506.

Figure S4.

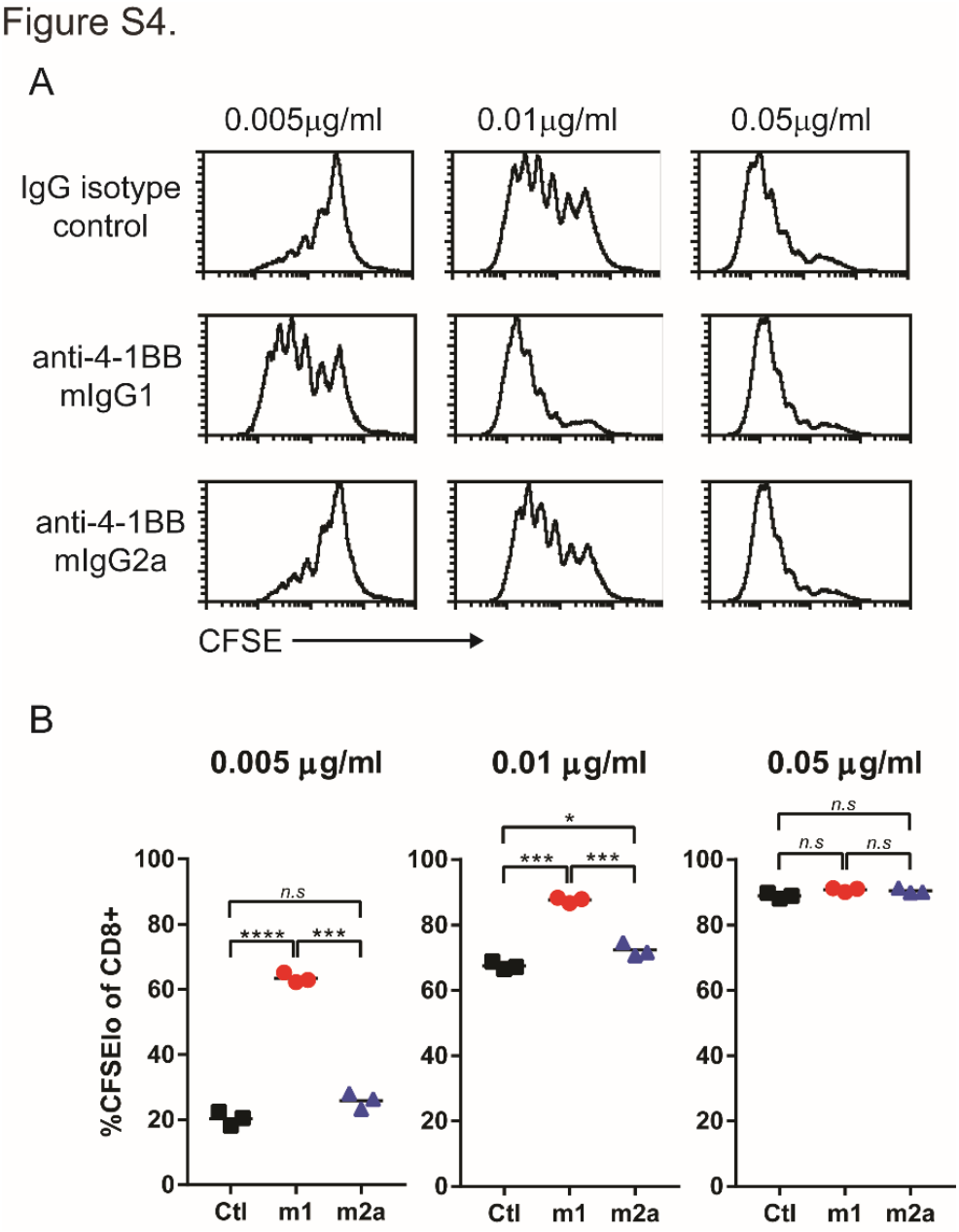

Figure S4, related to Figure 5. Anti-4-1BB mIgG1 exerts superior agonist activity compared with mIgG2a in vitro. (A) Splenocytes were isolated from C57BL/6 mice, labelled with CFSE and incubated with the concentrations of anti-CD3 indicated above and with 10 μg/ml anti-4-1BB mAb or control mAb. On day 3 cells were stained with anti-CD8 and CFSE visualized by flow cytometry. (B) Frequency of CFSElo cells within the CD8+ population from individual mice. Data are representative of two experiments.

Figure S5.

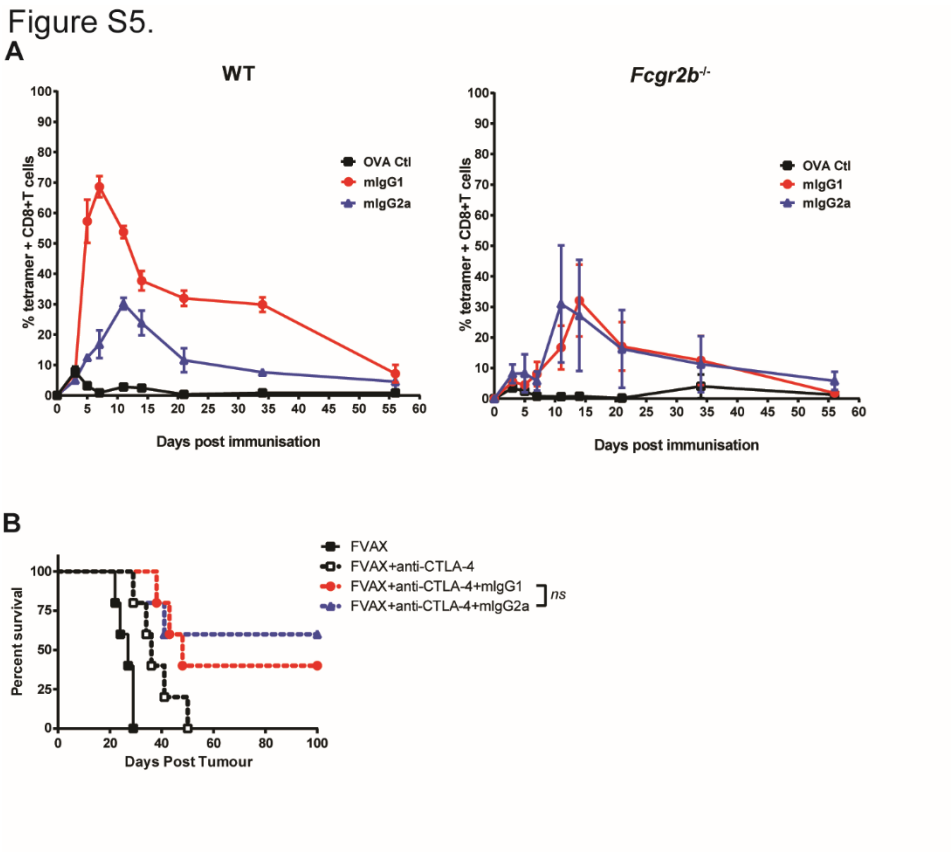

Figure S5, related to Figure 5. Anti-4-1BB mIgG1 and mIgG2a are equally therapeutic in the absence of FcγRIIB or in a vaccination setting. (A) Groups of 3 wild-type (left) or *Fcgr2b*$^{-/-}$ (right) mice received 2 × 10^5 OT-1 cells i.v., followed 24 hours later (day 0) by i.p. injection of 0.5 mg OVA and 200 μg mIgG1 or mIgG2a anti-4-1BB. Control mice received OVA alone. Blood samples were taken to measure circulating SIINFEKL tetramer+ CD8+ cells over the course of the response, expressed as a % (mean ± SEM) of total CD8+ cells. Data are representative of 2 experiments. (B) Groups of 5 C57BL/6 mice were injected with 2.5 x 10^5 B16/BL6 cells i.d. on day 0 prior to receiving 1 x 10^6 irradiated FVAX cells i.d. on the opposite flank on days 3, 6 and 9. Concurrent with FVAX injection mice received either PBS, 100 μg anti-CTLA-4 (clone 9D9) or anti-CTLA-4 and 300 μg anti-4-1BB antibodies as indicated i.p. Percentage survival to the humane end point is shown.

Figure S6.

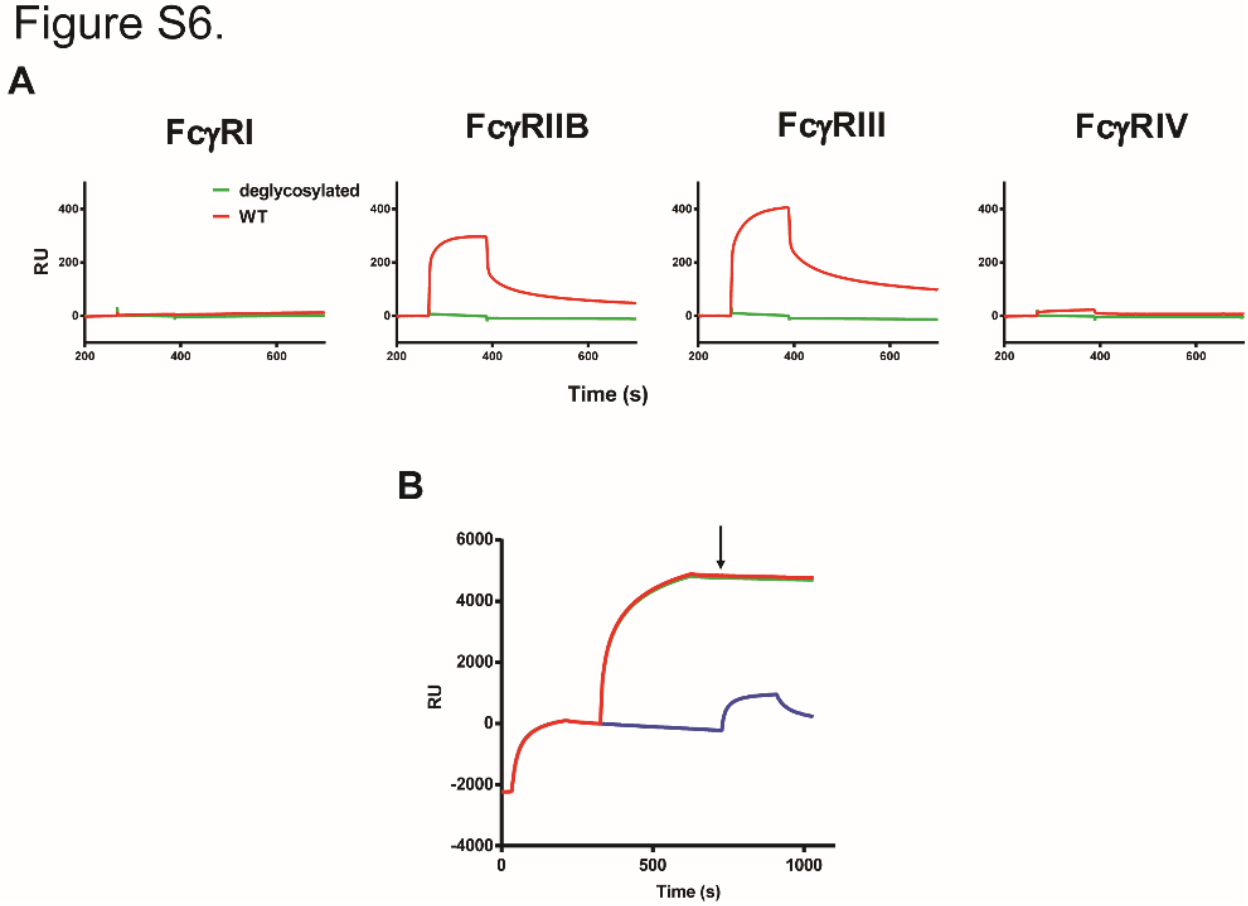

Figure S6, related to Figure 6. Anti-PD-1 mAb characterization. (A) Surface plasmon resonance analysis of anti-PD-1 (clone EW1-9) rIgG1 (red) and rIgG1 deglycosylated (green) binding to mouse FcγRI, IIB, III and IV. PD-1 mAb (500 nM) was passed over recombinant FcγR-his protein (1000 RU) (R&D Systems) captured onto a CM5 chip with an anti-histidine mAb (GE Healthcare). Sensorgrams are shown with 0 nM curve subtracted. (B) Analysis demonstrating that anti-PD-1 mAb bind to PD-1 and block PD-L1 binding. Anti-PD-1 rIgG1 (red), rIgG1 deglycosylated (green) or buffer (blue) was passed over recombinant PD-1-his (R&D Systems) (2000 RU) captured onto a CM5 chip with an anti-histidine mAb. At the time point indicated by the arrow recombinant PD-L1-Fc (R&D Systems) was passed over to demonstrate binding to PD-1 and blockade by anti-PD-1.

Figure S7.

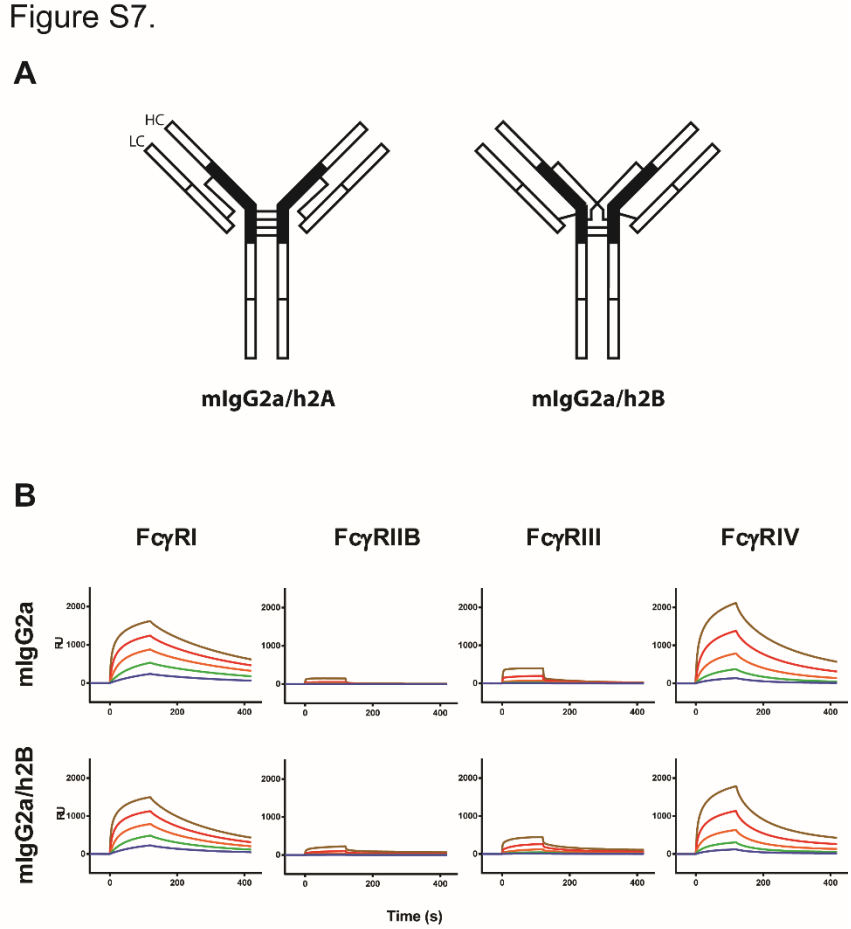

Figure S7, related to Figure 7. Anti-4-1BB mIgG2a/h2 disulfide isoforms and mIgG2a/h2B FcγR binding. (A) Schematic detailing disulfide bond arrangements in human CH1 and hinge region determining the nonagonist A and FcγR independent agonistic B structural isoforms. Figure based on (Wypych et al., 2008). (B) Surface plasmon resonance analysis of anti-4-1BB (clone LOB12.0) mIgG2a and mIgG2a/h2B binding to mouse FcγRI, IIB, III and IV. Recombinant, soluble FcγR protein (0 - black, 6 - blue, 23 - green, 94 - orange, 375 - red, 1500 nM - brown) was passed over 4-1BB mAb immobilized at 5000 RU. Sensorgrams are shown.